AL-BALQA APPLIED UNIVERSITY

Hashemite Kingdom of Jordan

Scientific Research Support Fund

Jordanian Journal of Engineering And Chemical Industries

DECEMBER 2019 | VOLUME 02 | ISSUE 03

ISSN 2617 - 720X (Online)
ISSN 2616 - 9584 (Print)

JJECI

www.jjeci.com

info@jjeci.com

An International Peer-Reviewed Scientific Journal Financed by the Scientific Research Support Fund

JORDANIAN JOURNAL OF ENGINEERING AND CHEMICAL INDUSTRIES (JJECI)

Jordanian Journal of Engineering and Chemical Industries (JJECI) is an international quarterly peer-reviewed research journal issued by the Scientific Research Fund, Ministry of Higher Education and Scientific Research, Amman, Jordan. JJECI is published by the Deanship of Research, Al-Balqa Applied University, Al-Salt, Jordan. The Journal publishes new and original Research Articles, Short Communications, Technical Notes, Feature Articles and Review Articles encompassing all fields of industrial and chemical engineering fields.

AIMS AND SCOPE

The Journal focuses on broad field of chemical engineering and industrial applications in which original contributions in the following areas appear
Physical Properties and Physical Chemistry
Transport Phenomena and Fluid Engineering
Separation Engineering
Thermal Engineering
Chemical Reaction Engineering
Process Systems Engineering and Safety
Biochemical, Food and Medical Engineering
Nanotechnology
Mathematical Modeling and Computer Simulation
Materials Sciences and Engineering
Energy, Water, Environment and Engineering
Industrial Management and Economics
Oil and Gas Processing
Chemical Engineering Education
Quality control and Standardization
Extractive Metallurgy
Industrial Chemistry

Other related Topics in Chemical Engineering are also welcomed

JJECI ADDRESS

Website: www.jjeci.com
E-mail: info@jjeci.com
Address: Al-Salt, Prince Ghazi Street
P.O.Box: Al-Salt, 19117 Jordan
Telephone: +962-5-3491111
Fax: +962-5-3532312

JORDANIAN JOURNAL OF ENGINEERING AND CHEMICAL INDUSTRIES (JJECI)

TYPES OF CONTRIBUTION

Research Paper: Manuscripts are not to exceed 5000 words excluding references as maximum limit to the length of the research paper including all text, figures, Table and references. It should include a set **of keywords and an abstract followed by Introduction, Materials and Methods, Results and Discussion, Acknowledgments, and References**.

Short Communication: deals with a concise study or preliminary findings that indicate an innovative piece of research that could be less substantial than a full research paper. Short Communication is limited to 2000 words. It should include a set of keywords, an Abstract and a 'Results and Discussion' Section (should be combined) and followed by Conclusion. The number of references is limited to 20 and the number of figures and/or tables is limited to 3.

Letter: Description of novel finding that might not be suitable for a regular research paper or short communication. Letter is limited to 1000 words. The number of references is 10 and the number of figures and/or tables is 2, and 10 references.

Review or mini-review: invited reviews should be of high interest to the readers of the scientific community.

JORDANIAN JOURNAL OF ENGINEERING AND CHEMICAL INDUSTRIES (JJECI)

AIM AND SCOPE:

Jordanian Journal of Engineering and Chemical Industries (JJECI) is an international quarterly peer-reviewed research journal issued by the Scientific Research Fund, Ministry of Higher Education and Scientific Research, Amman, Jordan. JJECI is published by the Deanship of Research, Al-Balqa Applied University, Al-Salt, Jordan. The Journal publishes new and original Research Articles, Short Communications, Technical Notes, Feature Articles and Review Articles encompassing all fields of industrial and chemical engineering fields.

The Journal focuses on broad field of chemical engineering and industrial applications in which original contributions in the following areas appear:

Physical Properties and Physical Chemistry
Transport Phenomena and Fluid Engineering
Separation Engineering
Thermal Engineering
Chemical Reaction Engineering
Process Systems Engineering and Safety
Biochemical, Food and Medical Engineering
Nanotechnology
Mathematical Modeling and Computer Simulation
Materials Sciences and Engineering
Energy, Water , Environment and Engineering
Industrial Management and Economics
Oil and Gas Processing
Chemical Engineering Education
Quality control and Standardization
Extractive Metallurgy
Industrial Chemistry

Other related Topics in Chemical Engineering are also welcomed

JORDANIAN JOURNAL OF ENGINEERING AND CHEMICAL INDUSTRIES (JJECI)

Preparation of Manuscripts

Manuscripts must be written in English typed in one columns fifty-seven lines on numbered pages of A4 or US letter size. All figures and tables should be included in the most appropriate locations within the main text, and not placed on separate pages. A corresponding author will be requested to consent to an agreement transferring copyright on behalf of all authors. All authors will be requested to consent to agreements of submission and authorship.

All authors are encouraged to register or add their ORCID ID when submitting their manuscript or creating their account. The ORCID ID will appear in the published manuscript if an author registers or adds their ORCID ID. Please visit http://www.orcid.org to learn more.

1)Title and authors: This should contain the following items in the given order.

i) Title: The title is to be written in 16 pt. Arial font, centered and using the bold and "Capital Caps" formats. There should be 24 pt. (paragraph) spacing after the last line

ii) Author's names (given name, and surname), affiliations and addresses. If authors' affiliations differ, these should be identified by use of superscripts 1, 2, etc. Identify the corresponding author and give the telephone number, fax number and e-mail address.

iii) If the research has been presented in part at a meeting, give the name, place and date of the meeting.

2) Abstract:

A brief summary (less than 300 words for research papers and journal reviews and 150 words for other types of papers, significant results and conclusions, followed by five keywords. Each keyword should consist of no more than three words.

1) Main Text: main headings will be followed after abstract and keywords by Introduction, Materials and Methods, Results and Discussion, Acknowledgments, and References. Leave a blank line above and below each main heading.
Equations: Number of equations in order with parentheses. Cite as Eq. (1), Eqs. (3) and (5). Spell out "Equation" if at the beginning of a sentence.
Figures and Tables: Each figure and table must have a caption. Cite as Fig. 1, Fig. 2 and 3, and Table 1. Color reproduction will be provided at no cost, if it is essential to clarify the description.

Literature: Cite in the text as follows: Matouq and Tagawa (1960), Matouq and Goto (1989a, 1989b), (Carslaw and Jaeger, 1960), and (Tan and Liou, 1989a, 1989b)
Units: The use of SI units is recommended.
Examples: k[W/(m K)] or k[$Wm^{-1}K^{-1}$], k= 0.58 W/(m K) or k= 0.58 $Wm^{-1}K^{-1}$
Chemical Nomenclature: Use IUPAC or Chemical Abstract conventions.

4) Nomenclature: List symbols in alphabetical order with their definition and SI units. Greek letters, subscripts and superscripts should follow Roman symbols.
5) Literature Cited: Arrange in alphabetical order according to last name of first author, patentee or editor.

1. **Journal Article:** Matouq, M., T. Tagawa and S. Goto, "Micro-channel reactor with guideline structure for organic–aqueous binary system", *J. Chem. Eng. Japan*, **26**, 254–258 (1993)
2. **Book Reference:** Carslaw, H. C. and J. C. Jaeger; Conduction of Heat in Solids, 2nd ed., pp. 198-201, Clarendon Press, Oxford, U.K. (1960).
3. **Chapter in a Book Reference:** Misra NC, Misra S, Chaturvedi A. Carcinoma gallbladder. In: Johnson CD, Taylor I, editors. Recent advances in surgery. London: Churchill Livingstone. 1997; 69-87.
4. **Conference proceedings:** Harnden P, Joffe JK, Jones WG, editors. Germ cell tumours V. Proceedings of the 5th Germ Cell Tumour Conference, 2001 Sep 13-15. Leeds, UK. New York: Springer, 2002.
5. **Dissertation:** Borkowski MM. Infant sleep and feeding: a telephone survey of Hispanic Americans [dissertation]. Mount Pleasant (MI): Central Michigan University. 2002.
6. **Patent:** Primack, H. S.; "Method of Stabilizing Polyvalent Metal Solution," U.S Patent 4, 374,104 (1983),

SUBMISSION OF MANUSCRIPTS

The author must provide a detailed cover letter including a declaration that the work has not been published elsewhere. It is author's sole responsibility that articles publishing from institutions have necessary approvals if needed.

All the articles must be submitted to the email: info@jjeci.com. All the manuscripts submitted should be in the Word (docx, doc format) or PDF format.

Submission of a manuscript implies that it has not previously been published, and is not under consideration for publication elsewhere (except patent disclosure(s) of the author(s)). The Editorial Committee will withdraw a submitted manuscript and retract acceptance and the published article, if any misconduct of publication ethics, which are specified in Guidelines on Publication Ethics for the Journal.

Peer Review Processing:

All articles submitted will undergo double blind peer review processing to meet the international standards. The editor handles the complete editorial process of the articles and peer reviewers remain anonymous to the authors. Editor decisions are strictly followed for quality publications.

AFTER ACCEPTANCE

After acceptance, the author(s) cannot modify the submitted manuscript. Any changes must be addressed through the Editorial office. For the typesetting of the publication, authors will be requested to submit original text and figures online in separate files. All the figures should be of professional quality.

COPYRIGHT

Authors must agree to transferring copyright to the Jordan Journal of Industrial and Chemical Engineering. No article can be published without this agreement.

PROOFS AND REPRINTS

Electronic proofs will be sent as an E-mail attachment to the corresponding author as a PDF file. Page proofs are considered to be the final version of the paper. With the exception of typographical or minor clerical errors, no changes will be made in the paper at the proof stage. Authors will have free electronic access to the full text of the paper. Authors can freely download the PDF file from which they can print unlimited copies of their chapters. Hard copy of

journal issues of which the article appears in will be supplied free of charge to the corresponding author.

PUBLICATION ETHICS

1. **Ethical Standards: JJICE** adheres to the principles of transparency and best ethical practices in scholarly publishing as recommended by the international committees like COPE, DOAJ, OASPA, and WAME.

2. **Plagiarism: JJECI** has strict policies against plagiarism. During the submission, authors require to state that their work is not a copy of another published work and their article is not submitted elsewhere (in full or in part). **JJECI** cross checks every submission for the plagiarism misconduct. Any submission containing partially/completely plagiarized content is rejected immediately.

3. **Attribution Practice:** Citations must be attributed for previously published content. If the authors have used content from any previouslypublished work and fail to provide credit to original source then it will be considered as technical plagiarism and the manuscript might be rejected or retracted.

4. **Conflicts of Interest: JJECI** conduct double blind peer review process to avoid conflicts. The authors should hold responsibility in disclosing any conflicts of interest during article submission to avoid any potential conflicts of interest.

5. **Confidentiality Protection: JJECI** undertakes multiple measures to safeguard the confidentiality and integrity of the authors' work. Editors, peer reviewers and journal staff require maintaining the confidentiality of authors' work. It is ethically not acceptable to use or disseminate the unpublished work.

6. **Human and Animal Rights:** All articles published with **JJECI** must adhere to high ethical standards concerning human volunteers and animal welfare. For animal models and human volunteers ethical clearance letter and documents are required, if applicable.

7. **Consents/Instances:** Authors require obtaining consent for publication from all contributors and participants of the work. Authors must submit the clear statements regarding consents with original signature while submitting their work.

8. **Professional Conduct:** Editors, Reviewers, Authors and the journal staff are expected to adhere to the basic professional courtesy.

Reviewer Guidelines

Peer review is the system for evaluating the quality, validity, and relevance of scholarly research. The process aims to provide authors with constructive feedback from relevant experts which they can use to make improvements to their work, thus ensuring it is of the highest standard possible.

The Review Process

The steps below are the high-level steps in the review process.

Receive Invitation to review

- Accept Invitation
- Review Manuscript
- Submit Review

As a reviewer, you will be notified by e-mail of an invitation to review a manuscript.

- Only agree to review manuscripts for which they have the subject expertise required to carry out a proper assessment and which they can assess in a timely manner.
- Respect the confidentiality of peer review and not reveal any details of a manuscript or its review, during or after the peer-review process, beyond those that are released by the journal.

Double-check the manuscript title page and the Acknowledgments section to determine whether there is any conflict of interest for you (with the authors, their institution, or their funding sources) and whether you can judge the article impartially.

Abstract -Has this been provided (if required)? Does it adequately summarize the key findings/approach of the paper?

Length - Reviewers are asked to consider whether the content of a paper is of sufficient interest to justify its length. Each paper should be of the shortest length required to contain all useful and relevant information, and no longer.

Originality - Is the work relevant and novel? Does it contain significant additional material to that already published?

Presentation –Is the writing style clear and appropriate to the readership? Are any tables or graphics clear to read and labeled appropriately?

References -Does the paper contain the appropriate referencing to provide adequate context for the present work?

Once you've read the paper and have assessed its quality, you need to make a recommendation to the editor regarding publication. The specific decision types used by a journal may vary but the key decisions are:

Accept- if the paper is suitable for publication in its current form.
Minor revision- if the paper will be ready for publication after light revisions. Please list the revisions you would recommend the author makes.
Major revision- if the paper would benefit from substantial changes such as expanded data analysis, widening of the literature review, or rewriting sections of the text.
Reject- if the paper is not suitable for publication with this journal or if the revisions that would need to be undertaken are too fundamental for the submission to continue being considered in its current form.

In your comments intended for the author, do not make statements about the acceptability of a paper (see the next paragraph); suggested revisions should be stated as such and not expressed as conditions of acceptance. Organize your review so that an introductory paragraph summarizes the major findings of the article, gives your overall impression of the paper, and highlights the major shortcomings. This paragraph should be followed by specific, numbered comments, which, if appropriate, may be subdivided into major and minor points. (The numbering facilitates both the editor's letter to the author and evaluation of the author's rebuttal.) Criticism should be presented dispassionately; offensive remarks are not acceptable.

Sometimes you will be asked to review a paper when you do not have sufficient time available. In this situation, you should make the editorial office aware that you are unavailable as soon as possible. It is very helpful if you are able to recommend an alternative expert or someone whose opinion you trust.

If you are unable to complete your report on a paper in the agreed time-frame required by the journal, please inform the editorial office as soon as possible so that the refereeing procedure is not delayed. Make the editors aware of any potential conflicts of interest that may affect the paper under review. Decision of the Editorial Board is final regarding publication of any manuscript.

COPYRIGHT AGREEMENT

JORDANIAN JOURNAL OF ENGINEERING AND CHEMICAL INDUSTRIES (JJECI)

Please complete and sign the form and send it with the final version of your manuscript. It is required to obtain written confirmation from the authors in order to acquire copyrights for papers published in the Journal so as to index them to various repositories.

Title of paper:

_____
_____
_____

Author(s):

_____
_____
_____

The undersigned hereby transfers any and all rights in and to the paper, including, without limitation, all copyrights to the JJECI. The undersigned hereby represents and warrants that the paper is original, is not considered for possible publication elsewhere and that he/she is the author of the paper, except for material that is clearly identified as to its original source, with permission notices from the copyright owners where required. The undersigned represents that he/she has the power and authority to make and execute this assignment.
This agreement is to be signed by corresponding authors and on behalf of co-authors who have obtained the assent of the co-author(s) where applicable.

_____

Author's Signature and Date

_____

Typed or Printed Name

_____

Institution or Company

Jordanian Journal of Engineering and Chemical Industries (JJECI)

Cover Letter/Declaration Form

Date of Submission:

Name of Corresponding Author:

Contact Information of the Corresponding Author

Address:

Email:

Tel:

Article Type:

Manuscript Title:

On behalf of all the co-authors, I am submitting the enclosed manuscript for potential publication only in ***Jordanian Journal of Engineering and Chemical Industries (JJECI).*** I attest that this paper has not been published in whole elsewhere and is prepared following the instructions to authors. All authors have contributed to this manuscript, reviewed and approved the current form of the manuscript to be submitted.

Signature _____
Date_____

EDITOR'S NOTE

This issue is the third published issue by JJECI online and print, with a recognized quality of research covering other sectors in chemical industries. This issue has started its preparation for online publication since June 2018, the submitted manuscripts have undergone a strict review process in which, at least, and three specialized reviewers with well-recognized research track in the subject area reviewed each manuscript.

I would like to sincerely thank all authors who submitted their latest research work to JJECI. I also would like to thank all the reviewers of the Journal for their efforts to ensure a very high-quality review process while keeping a reasonable timeline for submitting their reviews and recommendations.

I hope to receive from all potential authors, readers, and researchers their opinions, suggestions, and comments at (info@jjeci.com). My colleagues in the Editorial Board and I are very willing to adopt new ideas and thoughts that may be sent to us to improve the content quality and journal presentation.

Editor-in-Chief

Prof. Dr. Mohammed Matouq
Al-Balqa Applied University, Al-Salt, December 2019

JORDANIAN JOURNAL OF ENGINEERING AND CHEMICAL INDUSTRIES (JJECI)

Table of contents

ISSN (online): 2617-720X
ISSN-L (print):2616-9584

Control of a Benchmark CSTR Using Feedback Linearization

Malek Hajaya[1*], Tamir Shaqarin[2]

[1)]*Civil Engineering Department, Tafila Technical University, Tafila, 66110 Jordan*

[2)]*Mechanical Engineering Department, Tafila Technical University, Tafila, 66110 Jordan*

Output regulation control for a CSTR benchmark problem is considered using a feedback linearization technique, where a linear control method is applied to the system for the purpose of maximizing the yield of a desired product at a specific operational temperature. Simulation results showed that the proposed feedback linearization-based controller strategy was successful in maintaining the desired product concentration at its set points, while maintaining the cooling jacket temperate fixed at all times, and the manipulated variables were maintained within their respective operational limits. The proposed feedback linearization-based controller provided very promising results, where it guaranteed a precise operation of the reactor with good performance in terms of a stable transition with no overshoot, and exhibited robustness by rejecting the tested disturbance in the form of a sinusoidal time variation in the reactant feed concentration.

Keywords: Process control, Feedback linearization, Klatt–Engell CSTR, State regulation

Introduction

Continuously Stirred Tank Reactors (CSTRs) are processing units that are commonly used in various continuous production, reaction-based, operations. Process related conditions and/or economic considerations require the operation of such reactors to be at an optimal point, where a desired product yield is maximized or the production cost is minimized (Edgar *et al.*, 2001). This feat requires maintaining a specific set of operational conditions that dictate the processes inputs and outputs (i.e. input-output constraints) is undertaken by process control. One of the most widely adopted benchmark problem for the aforementioned situation is the CSTR reactor model presented by Klatt and Engell (Klatt and Engell, 1993; Kroll and Schulte, 2014), which include the reaction scheme originally presented by van de Vusse (Van de Vusse, 1964). The Klatt and Engell reactor model includes a realistic process that includes temperature-sensitive, consecutive and parallel liquid phase reactions, under actual physical considerations (Kroll and Schulte, 2014).

In-process control, a CSTR represents an open, non-linear, reaction system model that has balance equations that combine kinetics and hydrodynamics. A variety of approaches are proposed for the control of the aforementioned benchmark problem in the literature: Chen et al (Chen *et al.*, 1995) used nonlinear predictive control to maintain the operation of the CSTR at a desired set point by considering a multi-input and single-input control problems. Klatt and Engell (Klatt and Engell, 1998) have used the principle of gain-scheduling, while Rothfuss et al (Rothfuss *et al.*, 1996) used a flatness-based control approach. Graichen et al (Graichen *et al.*, 2004) and Perez et al (Perez *et al.*, 2002) introduced an inversion-based feedforward control design, while Kvasnica et al (Kvasnica *et al.*, 2010) proposed a method to approximate the nonlinear behavior of the system by several local linear models, thus allowing for a piecewise affine (PWA) model representation that predicted and optimized the reactor behavior. Abdalla and Shaqarin (Abdalla and Shaqarin *et al.*, 2017) have successfully implemented an alternative LMI (Linear matrix Inequality) approach on a CSTR for temperature and level control using LPV (linear parameter Varying) controller. In this work, state regulation control for the Klatt–Engell CSTR benchmark problem is considered using a feedback linearization technique, where a linear control method is applied to the system for the purpose of controlling the yield of a desired product at a specific operational temperature. Controlled and uncontrolled CSTR performance are compared at nominal conditions, and with an added disturbance in the reactant feed concentration. This alternative approach for state regulation control maintain the effect of the nonlinear part on the system's performance by using exact state transformations and feedback, rather than by linear approximations of the dynamics.

Received on July 2, 2019, accepted October 27, 2019. Correspondence concerning this article should be addressed to Malek G. Hajaya (E-mail address: mhajaya@ttu.edu.jo).ORCID ID for Malek G. Hajaya: https://orcid.org/0000-0003-0110-6731

1 Materials and Methods

1.1 The CSTR benchmark model

The benchmark model represents a constant volume CSTR with a constant volume. The reactions (Chen *et al.*, 1995; Rothfuss *et al.*, 1996) are taking place in the liquid phase, and represent the process of substance *B* production. This chain of irreversible reactions represents the production of Cyclopentenol (B) from Cyclopentadiene (A) via an acid-catalyzed electrophilic addition of water in dilute solution. Additionally, Dicyclopentadiene (D) is generated as a side product and Cyclopentanediol (C) as a consecutive product. **Figure 1** illustrates the CSTR reactor in the benchmark model, along with the variables used in the benchmark model.

$$A \xrightarrow{k_1} B \xrightarrow{k_1} C \quad (1)$$

$$2A \xrightarrow{k_2} D \quad (2)$$

where k_1 (1/hr) and k_2 (mol/m^3) are reaction rate constants for reactions 1 and 2. Reactant *A* is used to produce *B*, while undesired reactions take place producing two by-products (*C* and *D*) (Rothfuss *et al.*, 1996). Both steps of reaction 1 follow the same mechanism, thus the same reaction rate constant (k_1) is used for both steps (Klatt and Engell, 1993). As shown in the figure, the continuously mixed reactor, with an active volume of *V*, is fed by reactant *A* at a feed flow rate of Q_{in} (L/hr), a concentration of c_{Ain} (mol/m^3), and a temperature of T_{in} (^{o}C). The feed temperature is subject to variation. None of the products are present in the feed. The reactor effluent is at temperature T (^{o}C), with *A* and *B* concentrations of c_A and c_B (mol/m^3), respectively. Heat is removed by a rate of Q_H (kJ/hr) to maintain the exothermic reactions through the usage of a cooling jacket, which has a temperature of T_C (^{o}C), and an external heat exchanger.

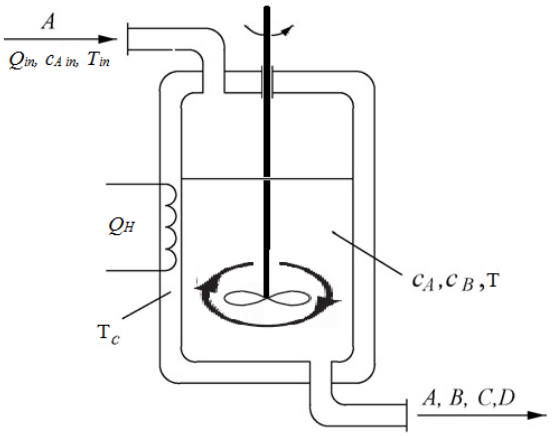

Fig. 1 Representation of the CSTR problem deferent variables.

Reactions rates for *A* and *B* are:

$$r_A = -k_1 c_A - k_2 c_A^2 \quad (3)$$

$$r_B = k_1 (c_A - c_B) \quad (4)$$

The dynamic behavior of the reactor can be represented by the material for *A* and *B*:

$$dC_A/dt = (\frac{Q_{in}}{V})(c_{Ain} - c_A) - k_1 c_A - k_2 c_A^2 \quad (5)$$

$$dC_B/dt = -(\frac{Q_{in}}{V})c_B + k_1 (c_A - c_B) \quad (6)$$

In addition to the heat balance between the reactor and the cooling jacket:

$$dT/dt = (\frac{Q_{in}}{V})(T_{in} - T) - (\frac{1}{\rho Cp})(k_1 c_A \Delta H_{R_{AB}} + k_1 c_B \Delta H_{R_{BC}} + k_2 c_A^2 \Delta H_{R_{AD}}) + (T_C - T)(\frac{A_R K_W}{\rho Cp V}) \quad (7)$$

$$dT_C/dt = \frac{Q_H}{m_K C_{PJ}} + \frac{A_R K_W}{m_K C_{PJ}}(T - T_C) \quad (8)$$

where C_P is the heat capacity of the liquid phase of the reactor, ρ is the density of the liquid phase, $\Delta H_{R\,AB}$ is enthalpy of the $A \rightarrow B$ reaction, $\Delta H_{R\,BC}$ is enthalpy of the $B \rightarrow C$ reaction, $\Delta H_{R\,AD}$ is enthalpy of the $A \rightarrow D$ reaction, A_R is the surface area of the cooling jacket, K_W is the heat transfer coefficient for the cooling jacket, m_K is the coolant mass, and C_{PJ} is the heat capacity of the coolant. The reaction rates in Equations 3 and 4 are affected by temperature through the Arrhenius law:

$$k_i = k_i^0 \exp\left(\frac{E_i}{T+273.5}\right) \quad (9)$$

where i denotes reaction rate constants 1 and 2, k_i^0 is the collision factor for rate constant i, and E_i is the activation energy for each of the aforementioned reaction constants (Chen *et al.*, 1995). Concentrations of substances C and D (the by-products) are not considered in the context of the model, and they do not influence the dynamics of the process (Rothfuss *et al.*, 1996). **Table 1** illustrates the values for the different physical and chemical parameters in the benchmark model.

As it is shown in Table 1, values of the collision factors and Enthalpy's do indeed have some uncertainty. This work used values of the best estimate in the simulations.

Table 1 Values for the different physical and chemical parameters in the benchmark model (Chen *et al.*, 1995)

Symbol	Parameter	Value
V	Reactor Volume	0.01 m^3
C_p	Heat capacity of the liquid phase of the reactor	3.01 kJ/kg.K
ρ	Density of the liquid phase	934.2 kg/m^3
$\Delta H_{R\,AB}$	Enthalpy of the $A \rightarrow B$ reaction	4.2 ± 2.36 kJ/mol A
$\Delta H_{R\,BC}$	Enthalpy of the $B \rightarrow C$ reaction	-11.0 ± 1.92 kJ/mol B
$\Delta H_{R\,AD}$	Enthalpy of the $A \rightarrow D$ reaction	-41.85 ± 1.41 kJ/mol B
A_R	Surface area of the cooling jacket	0.215 m^2
K_W	Heat transfer coefficient for the cooling jacket	4032 kJ/hr.K.m^2
m_K	Coolant mass	5.0 kg
C_{PJ}	Heat capacity of the coolant	2.0 kJ/kg.K
k_1^0	Collesion factor for rate conatant 1	$1.287 \pm 0.04 \times 10^{12}$ 1/hr
k_2^0	Collesion factor for rate conatant 2	$9.043 \pm 0.27 \times 10^6$ m^3/mol-A.hr
E_1	Activation energy for rate conatant 1	-9758.3 K
E_2	Activation energy for rate conatant 2	-8560.0 K

1.2 The control problem

The control problem of the specific benchmark model CSTR in hand involves a constrained control problem of a Multi-input Multi-output (MIMO) coupled nonlinear system. Feedback linearization technique is a good candidate for such problem; since it is capable of canceling the nonlinearities (fully or partially) and/or to decouple the model equations. A state feedback controller can be designed based on the feedback linearized system.

1.3 Feedback linearization

Feedback linearization is a technique used for nonlinear systems control design. Basically, the nonlinear dynamics of the system to be controlled is algebraically transformed, fully, or partially into a linear one. This enables the usage of linear control techniques in the system's controller (Slotine and Li, 1991). The value of this approach, compared to conventional linearization, stems from the fact that feedback linearization is achieved by exact state transformations and feedback, rather than by linear approximations of the dynamics. Thus, maintaining the effect of the nonlinear part on the system's performance. The mechanistic approach used in feedback linearization, *i.e.*, canceling the nonlinearities and imposing a desired linear dynamics, can be simply applied to a class of nonlinear systems described by the so-called companion form. A system is said to be in companion form if its dynamics is represented by:

$$x^{(n)} = f(\mathrm{x}) + b(\mathrm{x})u \quad (10)$$

where u is the scalar control input, x is states, $x = [x, \dot{x}, ..., x^{(n-1)}]^T$ is the state vector, and f(x) and b(x) are nonlinear functions of the states. This form of a dynamic system model is unique in the fact that it is easily transformed into a linearized system via direct feedback linearization.

The companion from Equation 10 can be transformed to a state-space representation as follows.

$$\begin{bmatrix} \dot{x_1} \\ \dot{x_2} \\ \vdots \\ \dot{x_n} \end{bmatrix} = \begin{bmatrix} x_2 \\ x_3 \\ \vdots \\ f(x) + b(x)u \end{bmatrix} \quad (11)$$

The nonlinear state-space is easily transformed to linear one by selecting an appropriate control law in the form of:

$$u = \frac{1}{b}[v - f] \quad (12)$$

The closed-loop system now is transformed to an equivalent linear state-space equation as follows:

$$\dot{x}^n = v \quad (13)$$

where v is the linear control law that can be designed via, state-feedback control, optimal control, pole-placement, … *etc*. The result is a linear input-output map between the new input and the output. **Figure 2** illustrates the input state linearization general form.

The resulting system structure is unique and system-specific, and most of the process systems cannot be represented as such, for instance, the CSTR. Albeit, feedback linearization can be used to fully (Shaqarin and Abdalla, 2009) or partially (Shaqarin *et al.*, 2014) cancel the nonlinearity for CSTR model, and remove the coupling between the state variables, especially, the controlled variables.

In the CSTR problem case, the system state is x^T= [c_A, c_B, T, T_c]. Controlled state variables are the effluent substance B concentration (c_B) and the jacket temperature (Tc) (Rothfuss *et al.*, 1996). The cooling jacket temperature is controlled as a means to control the reactor temperature. The manipulated variables are the reactor volume normalized flow rate Q_{in}/V (1/hr), and the heat removal rate by the jacket of Q_H (kJ/hr). From an operational point, Q_{in}/V is manipulated by changing the flow rate into and from the reactor, while Q_H can be manipulated through changes in the coolant flow rate and/or using a multiple heat exchangers setup, to name some. However, these changes can be strictly performed within specific constraints dictated by the process itself. The constraints for the Klatt–Engell CSTR benchmark model manipulated parameters are shown in the next section.

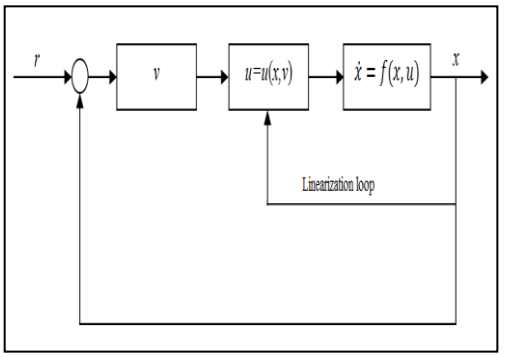

Fig. 2 General form for the input state linearization

1.4 CSTR operation

The state regulation problem requires operating the reactor at set points for substance B effluent concentration (c_B), while maintaining the temperature of the cooling jacket (T_C) at a desired value. **Table 2** shows the constraints on the state variables (for safe operation) and manipulated variables (Kvasnica *et al.*, 2010; Kroll and Schulte, 2014). In this work, the setpoints for c_B is 1.09 × 10^3 (mol/m^3), which is considered as the point where the maximum yield of B is obtained (Chen *et al.*, 1995). Values for the remaining model variables required to achieve this point (max yield) are shown in **Table 3**. The cooling jacket temperature is also regulated at 109 (^{0}C), which is lower than the temperature shown in Table 2. Finally, the CSTR model performance was simulated using MATLAB (The MathWorks Inc., Natick, MA).

Table 2 Constraints on the state variables and manipulated variables (Kvasnica *et al.*, 2010; Kroll and Schulte, 2014)

Model variable	Constraints
Q_{in}/V	5 to 35
Q_H	-8500 to 0
c_A	2.6 × 10^3 to 3.7 × 10^3 (mol/m^3)
c_B	0.6 × 10^3 to 1.1 × 10^3 (mol/m^3)
T	80 to 150 (^{0}C)
T_C	

2 Results and Discussion

2.1 Open-loop operation:

In order to validate the performance of the CSTR model, a simulation was performed for the maximum B yield point mentioned in Table 2. **Figure 3** illustrates four plots that represent the simulation result for an open, uncontrolled CSTR. Initial values for the model state variables in the reactor were assumed to be zero (c_A, c_B, T, and T_C= 0). After 2 hrs of simulated operation, effluent steady-state concentrations of A and B were 2.113× 10^3 and 1.09 × 10^3 mol/m^3, respectively, corresponding to a yield of 0.516 for B. Reactor and jacket steady-state temperatures were 114.25 and 112.93 ^{o}C, respectively. These results were identical to the values reported by Chen *et al.*, (1995) and Rothfuss *et al.*, (1996).

Table 3 Operational parameters at maximum, optimal, yield for B (Chen *et al.*, 1995).

Model inputs	Optimal value
c_{Ain}	5.1 × 10^3 (mol/m^3)
T_{in}	104.9 ^{0}C
Q_{in} / V	14.19 (1/hr)
Q_H	-1113.5 (kJ/hr)
c_A	2.14 × 10^3 (mol/m^3)
c_B	1.09 × 10^3 (mol/m^3)
T	114.2 ^{0}C
T_C	112.9 ^{0}C

In order to gain a better understating regarding the performance of the benchmark CSTR problem, multiple simulations were performed using values of the model's manipulated variables within the range depicted in Table 1. **Figure 4** shows four plots representing the resulted contour plot for the outcome of the simulation. The figure depicts how each of the state variables varies within the permissible range of the manipulated variables.

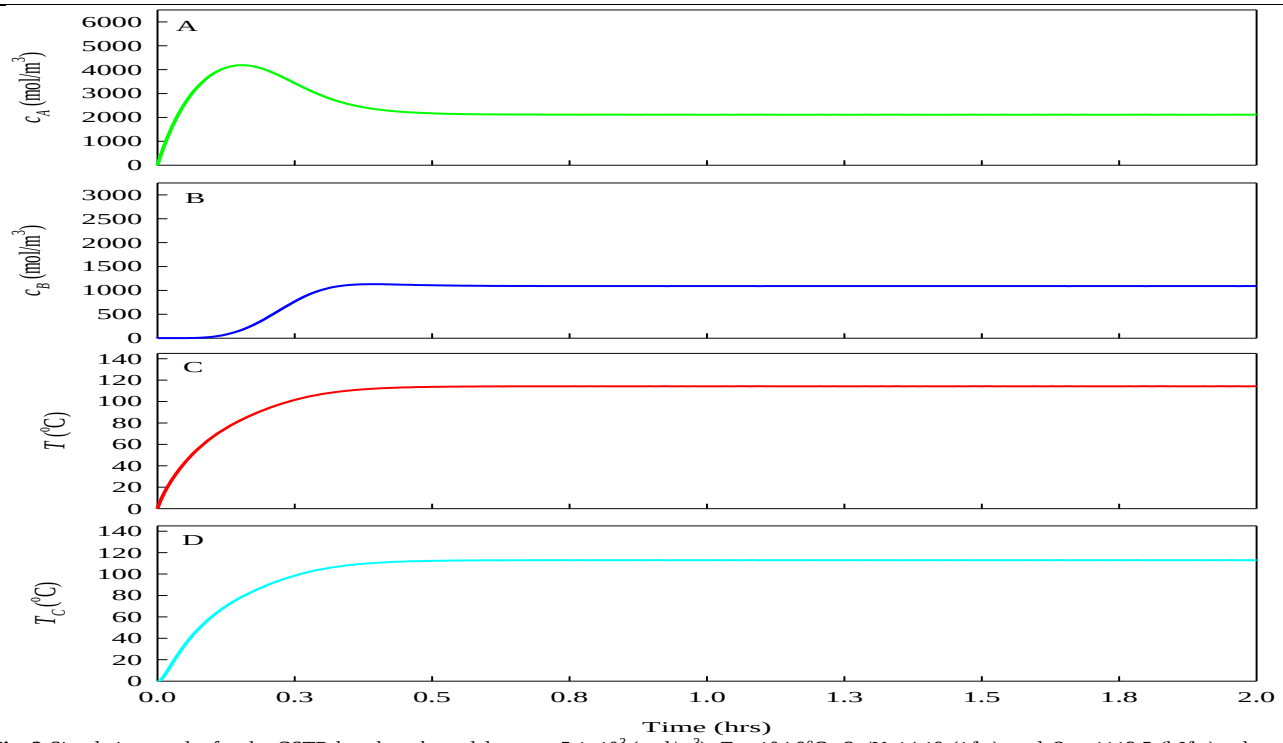

Fig. 3 Simulation results for the CSTR benchmark model at c_{Ain}=5.1x10^3 (mol/m^3), T_{in} =104.9°C, Q_{in}/V=14.19 (1/hr), and Q_H=-1113.5 (kJ/hr), where A: reactant A effluent concentration, B: Substance B effluent concentration, C: effluent stream temperature, and D: cooling jacket temperature.

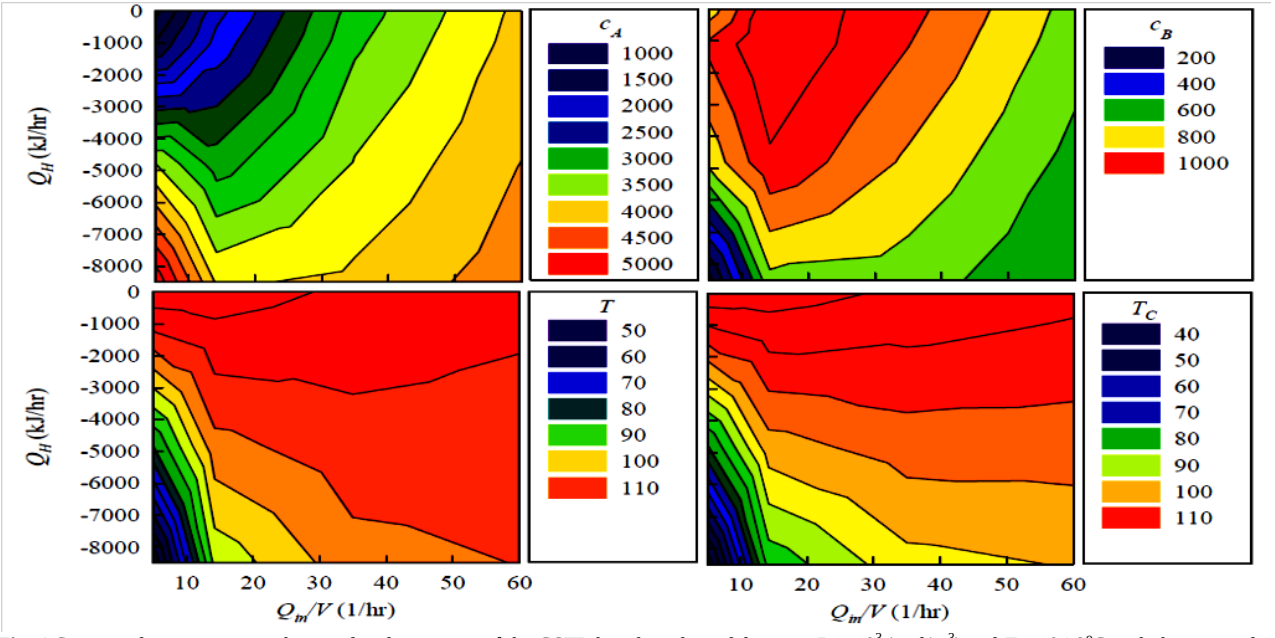

Fig. 4 Contour plot representing the simulated operation of the CSTR benchmark model at c_{Ain}=5.1x10^3 (mol/m^3) and T_{in}=104.9°C with the manipulated variables 5≤Q_{in}/V≤ 35 (1/hr), and -8500≤Q_H≤0 (kJ/hr).

As seen in the figure, the maximum concentration of B results from operating with a Q_{in}/V between about 9 and 25hr^{-1} and a Q_H between about -4200 and 0 (kJ/hr), while maintaining the constraints on the manipulated variables shown in Table 1. This range corresponded to a reactor temperature and a cooling jacket temperature between about 90 and 117^{0}C, which for the cooling jacket temperatures encompasses the desired set point for it at a temperature of 109^{0}C.

2.2 Output regulation Control

Typical simulations of the closed-loop nonlinear CSTR system response with feedback-linearization and state-feedback controller are discussed herein. The set-up understudy is to operate the reactor for the purpose of maximizing the yield of the

desired product B at a specific cooling temperature. Plots in **Figure 5** (solid lines) shows the controlled response of the CSTR model with feedback linearization for the operation at a set-point for c_B at $0.6x10^3$ and $1.09x10^3$ (mol/m^3), and a set-point for T_C at 109^{o}C, at inputs of c_{Ain}=$5.1x10^3$ (mol/m^3) and T_{in}=104.9^{o}C.

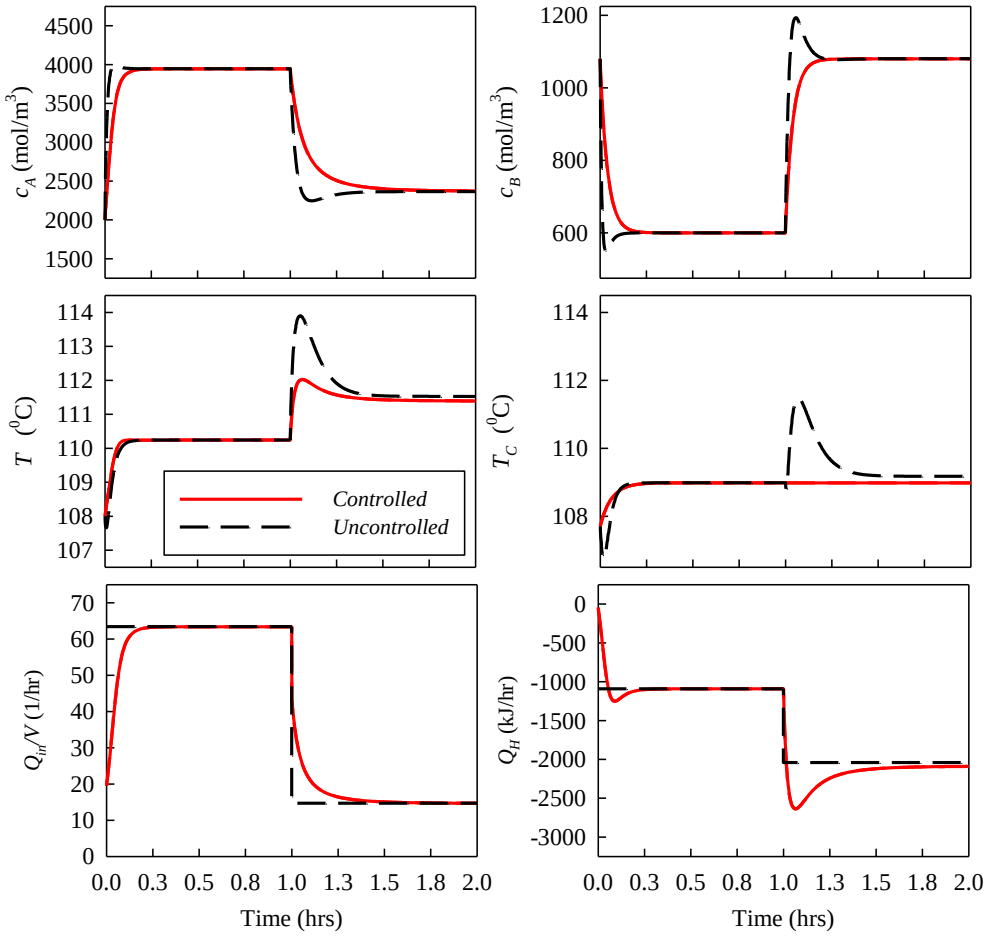

Fig. 5 Solid lines show the simulated controlled operation of the CSTR model with feedback linearization, with the set set-point for c_B at $0.6x10^3$ and $1.09x10^3$(mol/m^3), and T_C maintained at 109^{0}C, while dashed lines shows the simulated uncontrolled operation of the CSTR at values of Q_{in}/V and Q_H manually changed between 63.4 and 14.6 (1/hr) and -1090 and -2090kJ/hr, respectively; at c_{Ain}=$5.1x10^3$ (mol/m^3) and T_{in}=104.9^{0}C.

For this nominal scenario, as seen in the figure, the controller was able to regulate the operation of the CSTR, with a settling time of ≈ 0.2 (hr), to produce c_B at the desired maximum yield point. This was achieved by maintaining the desired T_c at the given set-point of 109 (^{0}C). The control effort remained within the constraints sanctioned on the system, changing Q_{in}/V between 63.4 and 14.6 (1/hr) and Q_H between -1090 and -2090kJ/hr. The same can be said for the remaining state variables, as they remained within the safe operation range (Table 1). The regulation of c_B at its maximum yield point was possible with a *Tc* value that is lower than the required temperature for optimal operation (Table 2). This was possible by increasing the heat removal rate at the jacket (Q_H), which increased from -1113.2kJ/hr, to -2090.8kJ/hr. This change slightly reduced the reactor temperature to 111.3^{0}C. On the other hand, values of Q_{in}/V settled back to a value that is almost identical to the optimal point (Table 2). The effectiveness of the proposed control technique can also be shown in **Figure 5** (dashed lines), where the simulated uncontrolled operation of the CSTR is depicted. This simulation was performed with the same input of c_{Ain}=$5.1x10^3$mol/m^3, and T_{in}=104.9^{o}C. Values of Q_{in}/V and Q_H were manually changed to mimic the range resulting from the controlled operation to be between 63.4 and 14.6 (1/hr) and -1090 and -2090kJ/hr, respectively. Compared to the controlled operation, the response of c_B and T_c reached and maintained their desired set points values. However, the controller allowed for a better performance in terms of overshoot and settling time for both outputs.

To test the robustness of the designed controller in disturbance rejection, the regulation control problem was simulated with sinusoidal disturbance as time variation in the inlet concentration substance *A* concentration (c_{Ain}) in the feed by ±100mol/m^3. Perturbations in $c_{A\,in}$ where achieved by changing its value to be: $c_{A\,in}$=5100+100 ×*sin* (8×*t*) (mol/m^3). Plots in **Figure 6** shows the

simulated controlled response (solid lines) and uncontrolled response (dashed lines) for the CSTR benchmark model with feedback linearization in the presence of the external disturbance (c_{Ain}).

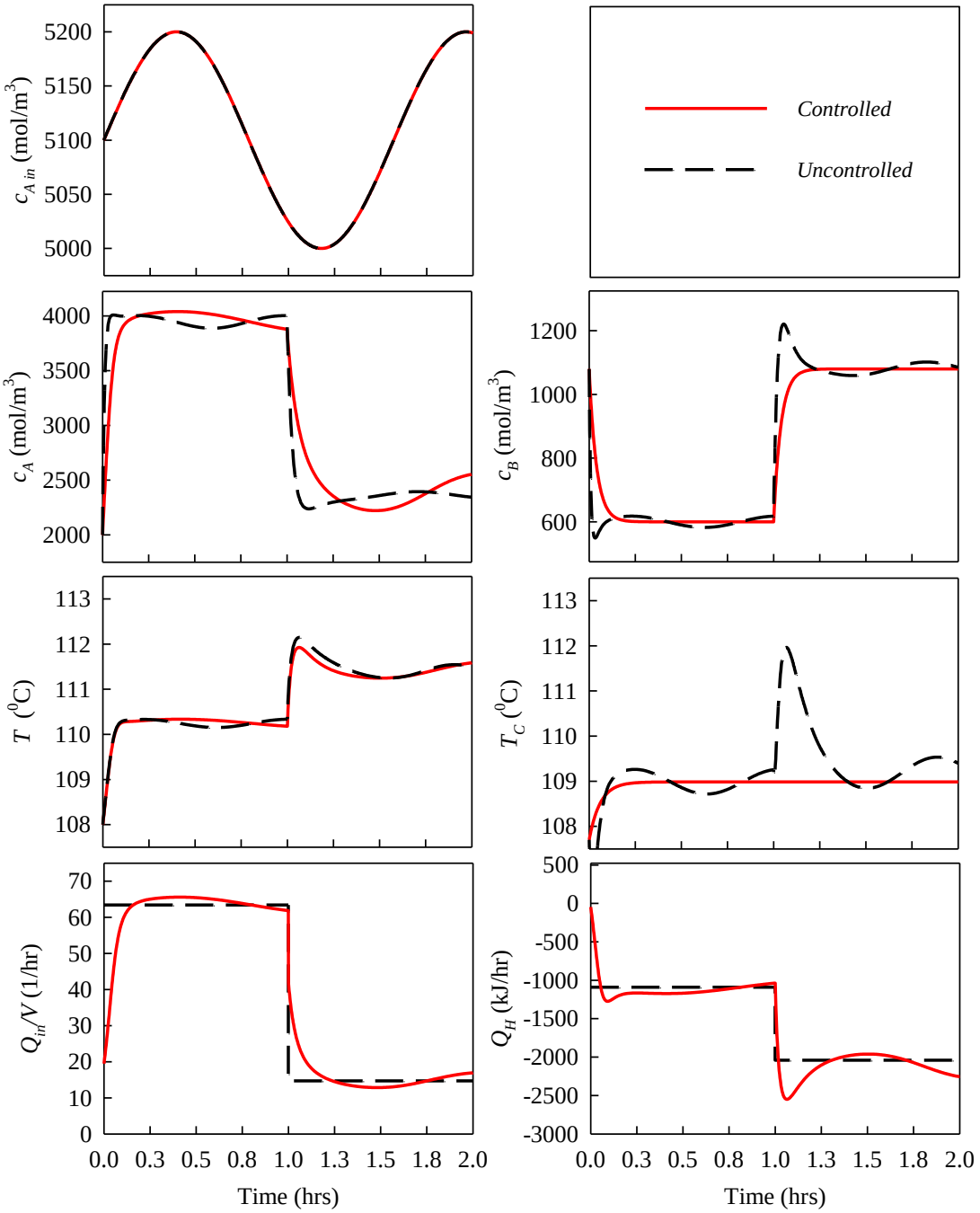

Fig. 6 Solid lines show the simulated controlled operation of the CSTR model with feedback linearization, with the set set-point for c_B at 0.6x10^3 and 1.09x10^3(mol/m^3), and T_C maintained at 109^{0}C, while dashed lines shows the simulated uncontrolled operation of the CSTR at values of Q_{in}/V and Q_H manually changed between 63.4 and 14.6 (1/hr) and -1090 and -2090kJ/hr, respectively; at c_{Ain}=5100+100sin (8×t) (mol/m^3) and T_{in}=104.9^{0}C.

Despite the external disturbance in the inlet reactant concentration in the CSTR feed, the controller was successful in regulating the outputs to the set-points. This observation leads to the conclusion that the controller is robust in disturbance rejection if it is found in the form of time variation of the inlet concentration. Compared to the controlled CSTR behavior, subjecting the uncontrolled CSTR to the same disturbance (dashed lines), resulted in a great degree of disturbance in the behavior of all the model outputs. This clearly shown in **Figure 6,** which shows how the outputs did not stabilize but rather contaminated with the same frequency of the external disturbance in c_{Ain}. Predictably, the current controller improved the performance significantly and was more robust against external disturbance compared to open-loop control.

Conclusions

This study aimed to introduce an alternative approach for controlling an of a complex, highly nonlinear, benchmark chemical reactor, that included a CSTR operating with temperature-sensitive, sequential and parallel reactions. Simulation results show that the proposed feedback linearization-based controller strategy was successful in regulating the desired product concentration to its set points while maintaining the cooling jacket temperate fixed at all times. The proposed feedback linearization-based controller provided very promising results. Not only does the controller guarantee a precise operation of the reactor, it also provided, compared to uncontrolled operation, improved performance in terms of settling time and overshoot. Disturbances in the feed reactant concentration did not affect the performance of the controller. The manipulated variables were maintained within the operational limit for each one of them, and the controller was robust against the tested external disturbance.

Nomenclature

Acronyms

CSTR Continuous stirred-tank reactor

Symbols

A:	=Reacting substance	[-]
B:	=Intermediate, desired product	[-]
C:	=Final product 1	[-]
D:	=Final product 2	[-]
k_1*:*	=Reaction 1 rate constant	[1/hr]
k_2*:*	=Reaction 2 rate constant	[m^3/hr.mol]
V:	=Reactor volume	[m^3]
Q_{in}*:*	=Feed volumetric flow rate into the reactor	[m^3/hr]
Q_H*:*	=Jacket heat removal rate	[kJ/hr]
c_{Ain}*:*	=Substance A concentration in the reactor feed	[mol/m^3]
c_A*:*	=Substance A concentration in the reactor and effluent	[mol/m^3]
c_B*:*	=Substance B concentration in the reactor and effluent	[mol/m^3]l]
T_{in}*:*	=Reactor feed temperature	[^{o}C]
T:	=Reactor and effluent temperature	[^{o}C]
Tc:	=Cooling jacket temperature	[^{o}C]
r_A*:*	=Overall reaction rate for A	[mol/hr.m^3]
r_B*:*	=Overall reaction rate for B	[mol/hr.m^3]
$\Delta H_{R\,AB}$*:*	=Enthalpy for the $A \rightarrow B$ reaction	[kJ/mol A]
$\Delta H_{R\,AC}$*:*	=Enthalpy for the $A \rightarrow C$ reaction	[kJ/mol A]
$\Delta H_{R\,BC}$*:*	=Enthalpy for the $B \rightarrow C$ reaction	[kJ/mol B]
C_P*:*	=Heat capacity of the liquid phase of the reactor	[kJ/kg.K]
C_{PJ}*:*	=Heat capacity of the liquid coolant	[kJ/kg.K]
A_R*:*	=Surface area of the cooling jacket	[m^2]
K_W*:*	=The heat transfer coefficient of the cooling jacket	[kJ/hr.K.m^2]
m_K*:*	=Coolant mass	[kg]
k_1^0*:*	=collision factor for rate constant 1	[1/hr]
k_2^0*:*	=collision factor for rate constant 2	[m^3/hr.mol]
E_i*:*	=Reaction *I* activation energy	[K]
x:	=State variables vector	[-]
f and b:	=Functions	[-]

Greek letters

ρ:	=Density of the reactor liquid phase	[kg/m^3]

References

Abdalla, M. and Shaqarin, T. “Industrial Process Control Using LPV”, *Modern Applied Science*, **11** (9), 39-50.(2017).

Chen, H., Kremling, A., and Allgöwer, F. (1995). Nonlinear predictive control of a benchmark cstr. pp. 3247-3252 P*roceedings of 3rd European control conference*.

Edgar, T.F., Himmelblau, D.M. and Lasdon, L.S.; "Optimization of chemical processes", *McGraw-Hill*, (2001).

Favache, A. and Dochain, D. "Thermodynamics and chemical systems stability: The cstr case study revisited", *Journal of Process Control*, **19**, 371-379.(2009).

Graichen, K., Hagenmeyer, V. and Zeitz, M. "Van de vusse cstr as a benchmark problem for nonlinear feedforward control design techniques", *IFAC Proceedings Volumes*, **37**, 1123-1128.(2004).

Graichen, K., Hagenmeyer, V. and Zeitz, M. "Design of adaptive feedforward control under input constraints for a benchmark cstr based on a bvp solver", *Computers & Chemical Engineering*, **33**, 473-483.(2009).

Gujer, W.; "Systems analysis for water technology", Berlin, Germany., *Springer*, (2008).

Klatt, K.-U. and Engell, S. "Rührkesselreaktor mit parallel-und folgereaktion", *VDI BERICHTE*, **1026**, 101-101.(1993).

Klatt, K.-U. and Engell, S. "Gain-scheduling trajectory control of a continuous stirred tank reactor", *Computers & Chemical Engineering*, **22**, 491-502.(1998).

Kroll, A. and Schulte, H. "Benchmark problems for nonlinear system identification and control using soft computing methods: Need and overview", *Applied Soft Computing*, **25**, 496-513.(2014).

Kvasnica, M., Herceg, M., Čirka, Ľ. and Fikar, M. "Model predictive control of a cstr: A hybrid modeling approach", *Chemical papers*, **64**, 301-309.(2010).

Perez, H., Ogunnaike, B., and Devasia, S. (2002). Output tracking between operating points for nonlinear processes: Van de vusse example. pp. 3281-3286 *Proceedings of the 2002 American Control Conference (IEEE Cat. No. CH37301)*, IEEE.

Rothfuss, R., Rudolph, J. and Zeitz, M. "Flatness based control of a nonlinear chemical reactor model", *Automatica*, **32**, 1433-1439.(1996).

Shaqarin, T, and Abdalla. M. "Simultaneous control of liquid level and temperature using feedback linearization techniques", *Proceedings of the 20th IASTED International Conference.* **670** (814), 71 (2009).

Shaqarin, T., N. Alshabatat, N., and B.R. Noack."Stabilizations of strange attractors by feedback linearization", *Research Journal of Applied Sciences, Engineering and Technology*, **8** (1), 43-47. (2014)

Slotine, J.-J.E., and Li, W.; "Applied nonlinear control", *Prentice Hall Englewood Cliffs, NJ*, (1991).

Van de Vusse, J. "Plug-flow type reactor versus tank reactor", *Chemical Engineering Science*, **19**, 994-996.(1964).

Theoretical Study of Photovoltaic Thermal Integrated Absorption Cooling System under Jordan Climate

Mohammed Al-Odat*[1], Mohamad Okour[1], Ahmed Dawahed[2], Isam Qasem[1], Fayez Elessa[1]

[1)] *Mechanical Engineering Department- Al-Huson University College-Al-Balqa Applied University, Irbid-Jordan*

[2)] *Mechanical Engineering Department- Jordan University of Science and Technology Irbid-Jordan*

This paper presents a theoretical investigation to simulate the utilization of (PV/T) technology to drive an absorption refrigeration system that is used for air conditioning of a classroom under Jordan climate conditions. The absorption refrigeration cycle uses the hot water from the PV/T collector with an assisted electrical heater as a heat source in the generator. In addition to the capability to utilize the PV/T to supply the building by domestic hot water and electricity if no need to run the refrigeration cycle. This analysis was carried using excel program and theoretical equations for the system. It was found that (PV/T) technology is very useful for thermal applications with high efficiency. Also, absorption refrigeration cycle has a good coefficient of performance because it mainly depends on the thermal energy with low electrical energy consumption to run the pump. Moreover, this system has a short payback period, low energy consumption, low running cost, and minimum environmental impact. The results of this study show that the system needs about (84 m^2 PV/T collectors) to cover 16 tons cooling load.

Keywords: Solar radiation, PV/T cell, thermal efficiency, electrical efficiency, absorption refrigeration, numerical solution

Introduction

Energy production, efficient use for energy and environmental impact become one of the main problems in the world; developing different renewable energy recourses (such as solar energy, wind energy, hydraulic energy …etc.) can contribute to overcome these problems. Solar energy is one of the most important renewable energy resources due to its large amount and its availability. Solar energy, in general, can be utilized in two methods: first, the solar thermal power that can be employed as heating energy by different types of solar thermal collectors that convert solar thermal energy to thermal heat. Second, converting the solar light energy directly to electricity using solar photovoltaic technology. This research work addresses a new technology called thermal photovoltaic collector which is a cumulative technology between photovoltaic modules and solar thermal collectors (Bhargava *et. al*. 1993). Thermal photovoltaic (PV/T) collectors is a new technology which used to utilizing the solar thermal and electrical energy simultaneously, this system depends on single crystal solar cells to convert solar light to produce electricity and embedded solar collector in the module used to absorb solar thermal heat energy from solar radiation by transfer the heat from absorption plat to working fluid in collector, also the working fluid in collector will make a good role to cool the cells which leads to increase the efficiency of the solar module. New PV technology developed in the last decade like organic PV cells, fixable PV (Pagliaro et. al. 2008). The thermal PV system is classified according to the PV/T design and cooling liquid PV/T collector, air PV/T collector and concentrated PV/T collector (Tyagia *et. al* 2012). Concentrating photovoltaic technology is one of the fastest-growing solar energy technologies, electrical conversion efficiency can reach more than 43%. The operating temperature of a solar cell strongly influences the performance of a photovoltaic system reducing its efficiency with a negative temperature coefficient. Thus, cooling systems represent a very important aspect in photovoltaic applications (Micheli *et. al* 2013, Brinkworth and M. Sandberg 2006). Many applications are developed to utilize the PV/T such as employing the generated hot water from collector for cooling in the absorption system (Gur Mittelman et. al 2007) or direct utilization as a domestic hot water (Vokas et. al 2006). In addition, PV/T can be used in the water desalination systems (Mittelman2009, Kumar and Tiwari 2008). The air PV/T type can be utilized to preheat the ventilating air (Twinsolar 2010) or for space heating (Ji J, et al 2009), also some research was tried to use the air PV/T for crop drying (Tiwari *et. al.* 2009) and marine drying (Fudholi *et al* 2010). A new idea for using the PV/T in hydrogen production is reported by Ratlamwalam (2011). Absorption refrigeration cycle is system generally consist of two evacuated containers: the first one contains a liquefied refrigerant which will be used in the refrigeration cycle. The second one contains the absorption liquid, this liquid will absorb the refrigerant liquid until reach saturation, and then this homogeneous solution will be pumped. The solubility of absorption liquid in refrigerant fluid will be reduced by heating. Finally, the produced refrigerant will be taken to complete the ordinary refrigeration cycle (Assilzadehet al 2005). Thus the system depends on the thermal heat energy supplied by the thermal photovoltaic collector using a water as a cooling fluid for the cell, and an auxiliary heater can be used to increase the water temperature to the obtain an optimum cycle performance. Also, this system can be used for lighting when there is no need to drive the refrigeration cycle.

Received on March 27, 2019; accepted on October 1, 2019 Correspondence concerning this article should be addressed to Mohammed Al-Odat (E-mail address: m.odat@bau.edu.jo).ORCiD ID of Mohammed Al-Odat https://orcid.org/0000-0002-2877-1611

The system has many advantages such as supplying the building with domestic hot water and electricity and the system can be grid-connected if the electricity generated by the PV/T more than the building demands. Dai *et. al*. (2017) studied numerically a hybrid photovoltaic solar-assisted loop heat pipe/heat pump (PV-SALHP/HP) water heater system. Their system was a combination of loop heat pipe (LHP) mode and heat pump (HP) mode, and the two modes can be run separately or compositely according to the weather conditions. Recently, Dubey and Supinator (2018) analyzed a novel integrated solar photovoltaic–thermal–refrigeration (PVTR) system used to produce hot water and air-conditioning in the tropical climate conditions of Singapore. They formulate a dynamic simulation model for the analysis of the PV sandwich attached with a solar flat plate collector and for the main components of the refrigeration system. Most recently Ammar *et. al*. (2019) reported the energy and energy performance of a photovoltaic/thermal solar-assisted heat pump system (PV/TSAHPS) with different solar radiation levels. From the heat pump, the solar evaporator/collector extracts the thermal energy required, while the cooling effect of the refrigerant reduces the working temperature of the PV cells. The previous literature review shows that the application of this particular PV/T system for absorption refrigeration under Jordan climate conditions has not been investigated yet. This was the motivation of the present work. This study focus on cooling of classroom in Jordan University of Science and Technology by operating a single effect absorption refrigeration system with lithium bromide as a working fluid. This system needs a heat source to drive the refrigeration cycle. Thus a flat plat thermal photovoltaic collector PV/T is used to supply the absorption cycle by required heat to drive the cycle under Jordan climate. This work introduces a case study on the cooling a classroom in Jordan University of Science and Technology using proposed techniques along with an economic analysis and payback period calculations.

2. Materials and Methodology

An absorption cooling system was designed for cooling, this cooling absorption system needs a heat source to drive the refrigeration system. In this work, the heat source is supplied by a hot water stored in a storage tank connected to the output of the thermal flat plate of the PV/T system. The hot water is overheated by an auxiliary electrical heater that inserted in the storage tank to obtain the required temperature to drive the cycle efficiently as shown in **Figure 1**.

2.1 Thermal photovoltaic collector

Thermal photovoltaic collector is a new technology that can generate electricity from the solar cells in addition to hot water from thermal flat plate collector attached to the bottom of the PV cells, the thermal energy is generated from the solar radiation and from cooling of the PV cells (Tyagia *et. al.* 2012). It was found that cooling the PV cells leads to increase electrical efficiency (Ibrahim et. al. 2011). A water PV/T collector type used in this work is illustrated in Fig. 1. A PV/T analysis generally is a combined between a thermal flat plate collector and PV panel so a thermal and electrical analysis will be carried out for the PV/T system under consideration.

2.1.1Thermal analysis

The Reynolds and Nusselt number are given in equations (1) and (2) (Cengel *et. al.* 2011)

$$Re = \frac{\rho v D}{\mu} \quad (1)$$

$$Nu = 0.664 Re^{1/2} Pr^{1/3} \quad (2)$$

A heat transfer analysis is done for the thermal part of system molding and this is given by the following equations (Duffie and William 2013)

Thermal efficiency is given by equation (3)

$$\eta th = \frac{Qu}{GAC} \quad (3)$$

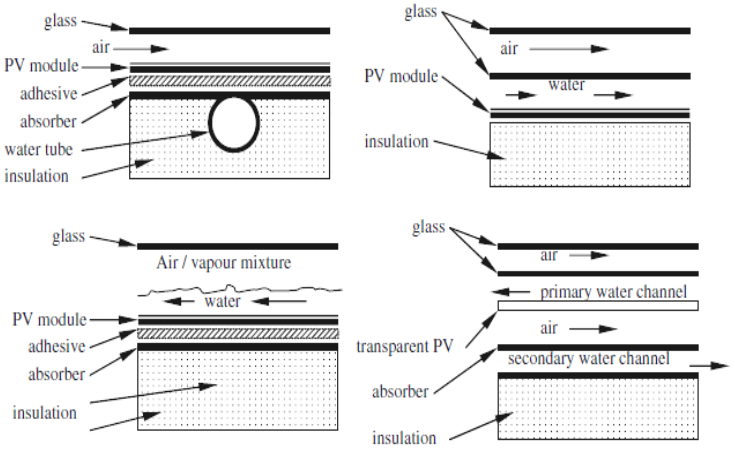

Fig. 1 Water-type PV/T cell.

The heat transfer coefficient of the heat losses from glass cover to the ambient hc,p_c is given by equation (4) which depends on Re and Nu.

$$hc,p_c = hw = \frac{Nu.D}{k} \quad (4)$$

The heat transfer coefficient for radiation heat loss from glass to the ambient hr,c_a is given in equation (5)

$$hr,c_a = \epsilon g\sigma(Tp + Ta)(Tp^2 + Ta^2) \quad (5)$$

And the heat transfer coefficient from plat to the glass hr,p_c is represented in equation (6)

$$hr,p\_c = \frac{\sigma(Tp+Ta)(Tp^2+Ta^2)}{\frac{1}{\varepsilon r}+\frac{1}{\varepsilon p}-1} \quad (6)$$

So the overall heat transfer coefficient Ul is calculated by equation (7)

$$Ul = \left(\frac{1}{(hc,p_c+hr,p_c)} + \frac{1}{(hw+hr,c_a)}\right)^{-1} \quad (7)$$

And collector efficiency factor *F'* is given by equation (8)

$$F' = \frac{1/_{Ul}}{W[\frac{1}{Ul[Do(W-Do)F]}+\frac{1}{cb}+\frac{1}{\pi Dihfi}} \quad (8)$$

Where

$$cb = \frac{kb}{\delta} \quad (9)$$

In equation (10) issued to fiend FR.

$$FR = \frac{\dot{m}cp}{AcUl}\left[1 - \exp\left(-\frac{UlF'Ac}{\dot{m}cp}\right)\right] \quad (10)$$

The fin efficiency factor F is calculated by equation (11)

$$F = \frac{\tanh(x)}{x} \quad (11)$$

Where x equal to

$$x = \sqrt{\frac{Ul}{k\delta}(\frac{W-Do}{2})} \quad (12)$$

$$Do = Di + t \quad (13)$$

For the heat transfer analysis for the plate collector to calculate the net heat gain by the collector *Qu* in equations (14) and (15)

$$Qu = AcFr[S - Ul(Ti - Ta)] \quad (14)$$

$$Qu = \dot{m}cp(To - Ti) \quad (15)$$

2.1.2 PV panel analysis

The electrical analysis is done for the PV/T panel firstly the electrical efficiency is given by equation (16)

$$\eta_{el} = \eta_o(1 - \beta[T - 25]) \quad (16)$$

And the cell PV panel temperature correlation is given by equation (17) (Lasnier and Ang, 1990).

$$T_{pv} = 30.0006 + 0.0175(G - 300) + 1.14(T_a - 25) \quad (17)$$

2.2 Absorption cycle

The working fluid in the absorption refrigeration cycle is a binary solution consisting of a refrigerant and an absorbent. A survey of absorption fluids provided by Marcriss suggests that there are some 40 refrigerant compounds and 200 absorbent compounds available cycle (Srikhirinet al. 2001). For the single effect absorption cycle Fig. (2), there are different input parameters (such as T_g, Tc, Ta, Te, EL, Q_E) that must be known in order to determine the thermodynamic properties at each stage in the cycle and amount of heat and mass flow rate in each component. The absorption cycle modeling depends on the thermodynamic and fluid analysis is given by the following equations (Srikhirin and Aphornratana, 2001).

Firstly, a Conservation of mass where the total mass input equal to the total mass output for each control volume in the system.

$$\Sigma \dot{m}i = \Sigma \dot{m}o \quad (18)$$

Conservation of energy where the total amount of energy input without energy generation equal to the total amount of energy output for each control volume in the system

$$Qin+\Sigma \dot{m}i.hi=\Sigma \dot{m}o.ho+Wout \quad (19)$$

Conservation of species where the total mass multiplied by the concentration input equal to the total mass multiplied by the concentration output for each control volume in the system.

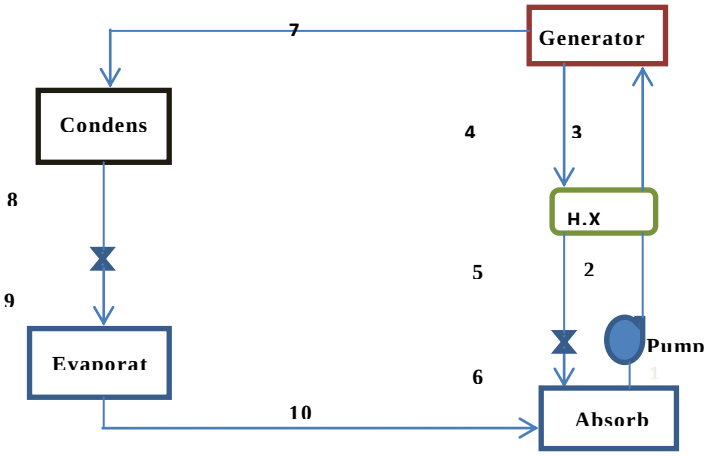

Fig. 2 Schematic diagram of single-effect absorption cycle

$$\Sigma \dot{m}i.Xi = \Sigma \dot{m}oXo \quad (20)$$

Coefficient of performance of the cycle equal ratio of the evaporator energy to the generator energy and pump work

$$Cop=\frac{Qe}{Qg+Wp} \quad (21)$$

2.3. System integration

The system integration is done by transfer the hot water from the flat plate PV/T to the storage tank and then increase the water temperature by an auxiliary heater driven by the PV/T panel electrical energy as shown in **Figure 3**.

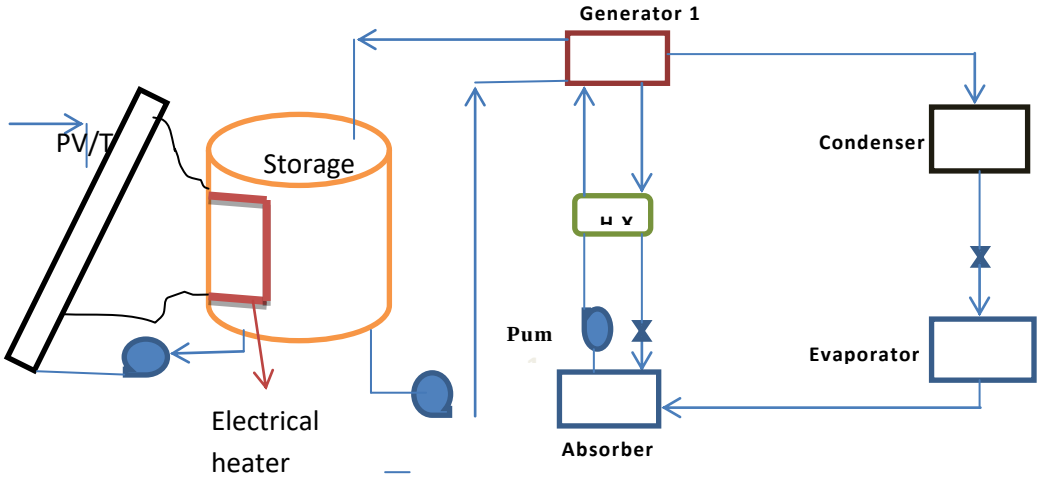

Fig. 3 Schematic diagram of the system

2.4 Simulation parameters

The simulation parameters are listed in **Table 1**. Numerous parameters that affect the system performance were investigated these parameters are wind speed, ambient temperature, generator and condenser temperatures, and the water mass flow rate.

Table 1 Simulation input parameters

Parameter	Value
Flat plate width(W)	0.5m
Water inlet temperature(Ti)	55°C
Emissivity of the glass (εc)	0.88
Emissivity of the plate(εp)	0.95
Fin thickness (δ)	0.5mm
Inner diameter of the tube (Di)	10mm
Outer diameter of the tube (Do)	12mm
Tube spacing (w)	150mm
Bond width(b)	2m
Fin thermal conductivity(k)	385W/m.k
For the absorption cycle:	
Evaporator temperature(Te)	7 (°C)
Absorber temperature(Ta)	40(°C)
Heat exchanger efficiency	0.8
Cooling load	16 ton

4. Results and Discussion

4.1 Solar radiation

The simulation has been carried utilizing MS Excel to solve the equations and investigate the effect of the variables mentioned in the above section. Figure 4 shows the variation of the measured solar for Irbid city in Jordan, this data was obtained from the energy center in Jordan University of Science and technology by a Pyranometer device. Figure 4 shows a normal distribution of solar radiation during the day in months from June to September, but there is a slight variation in the solar radiation in May and October. The slight variation of the solar radiation in May and October is due to the presence of some clouds that shaded the solar radiation from the Pyranometer.

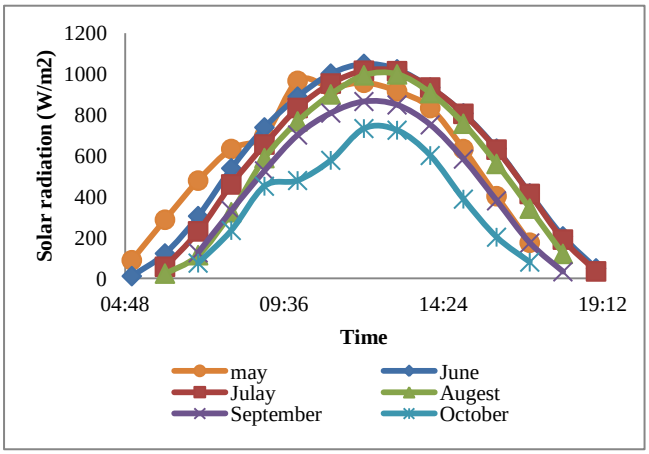

Fig. 4 Measured solar radiation in Irbid-Jordan for different months

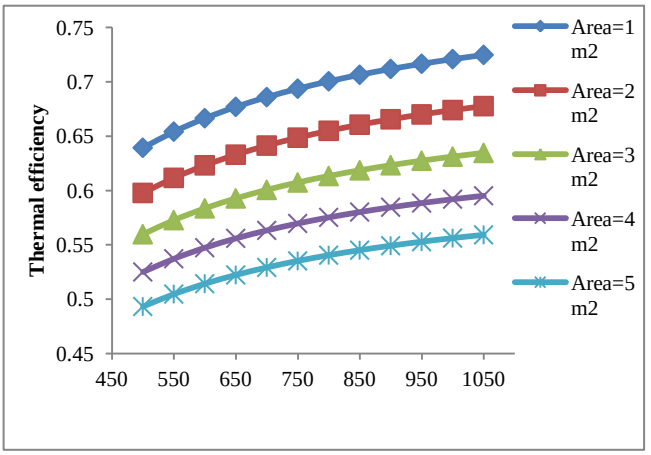

Fig. 5 Solar radiation effect on thermal efficiency of PV/T for various areas (Area is in m^2)

4.2 PV/T Performance Results

A thermal and electrical analysis was carried out for the PV/T collector, this analysis takes into consideration all the major parameters that affect the system performance. **Figure 5** shows the results of studying the effect of solar radiation intensity and the collector area on the thermal efficiency of the PV/T collector. It can be seen that the thermal efficiency of the PV/T increases as the solar radiation increases; this is due to an increase of the amount of input solar power to the collector which leads to an increase in its efficiency. In addition to is clear that the thermal efficiency of the PV/T collector increases by decreasing the collector area, this behavior can be attributed to the increase of the heat loss to the ambient with the increase in the area. **Figure 6** shows the effect of the wind speed on the thermal efficiency of the PV/T collector for various areas. It is obvious that as the wind speed increases the thermal efficiency of the PV/T decreases. This trend is attributed to the increase of the heat loss by the increase in the wind velocity due to the increase of the heat transfer coefficient hc,p_c between the plate and the ambient. The influence of the water mass flow rate on the thermal performance of the PV/T collector is displayed in **Figure 7**. It obvious that

the thermal efficiency of the PV/T increases as water flow rate increases until a specified flow rate, then the efficiency remains constant. This study was done for various areas and all show a similar trend, firstly as the mass flow rate increase that means an increase in the heat gain from the absorber to the water but after a specific value of mass flow rate, an increase in the mass flow rate doesn't affect the thermal efficiency.

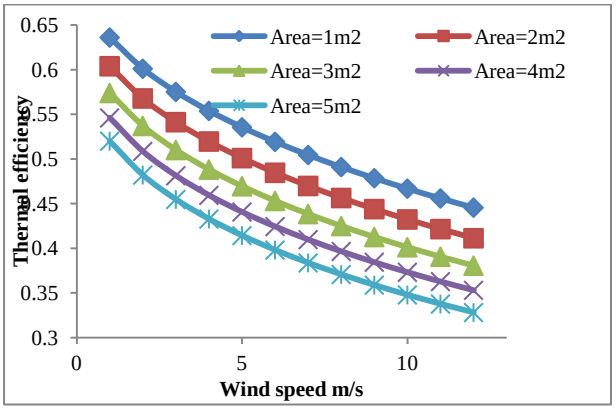

Fig. 6 Wind speed effect on the thermal efficiency of the PV/T for various areas (Area is in m^2)

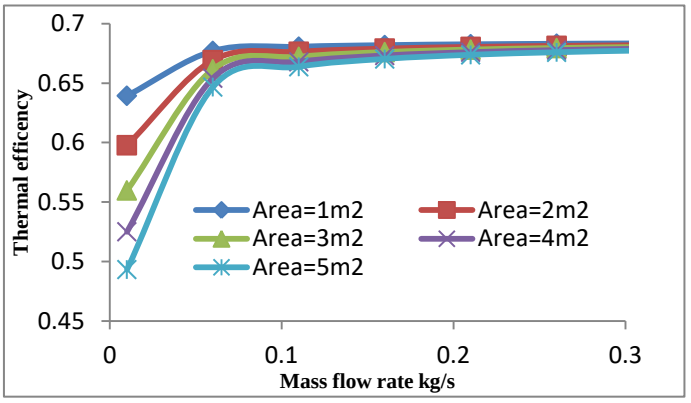

Fig. 7 Mass flow rate effect on the thermal efficiency of the PV/T for various areas (Area is in m^2).

The electrical efficiency of the PV/T cell is investigated taking into account the main parameter that affects PV cells efficiency which is the cell. Figure 8 shows the influence of the cell temperature on the PV/T cell's electrical efficiency. As shown in **Figure 8** an increase in the PV/T cells temperature leads to a decrease i the electrical efficiency of the PV/T cells during a day. This behavior is similar to the results reported by Swapnil and Dubey(2018). The total energy gain by the PV/T during the month of June solar radiation during the daytime for various ambient temperature is displayed in **Figure 9**. It can be seen that the energy generated by the PV/T increases as the solar radiation increases during the day. Although the PV/T cells efficiency decreases as the ambient temperature increases but the increase of the ambient temperature leads to the decrease of the thermal loss to the ambient which in turns increases the thermal efficiency, therefore, the total energy increases.

4.3 Absorption cycle

A numerical analysis was carried for the absorption refrigeration cycle. The effect of the generator temperature on the generator energy at different condenser temperature is shown in **Figure 10**. It can be seen that, as the generator temperature increases the generator energy decrease at the beginning due to increasing the coefficient of performance (COP). Continuing to increase in the generator temperature leads to the decrease of the COP so the generator temperature increase. Also as the condenser temperature increases the generator energy increases, because the increase in condenser temperature leads to reduce the amount of heat rejection from the condenser**.**

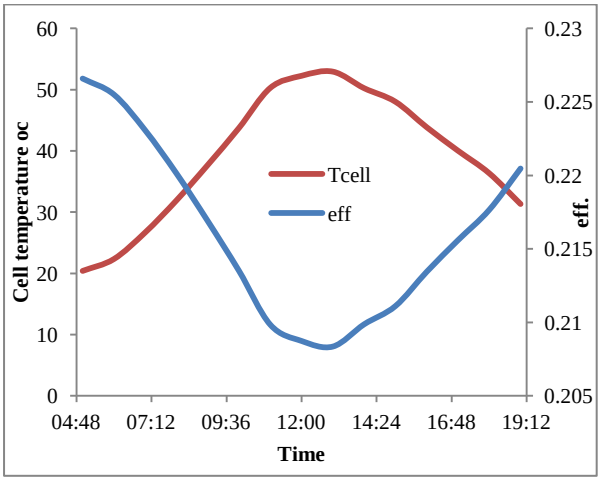

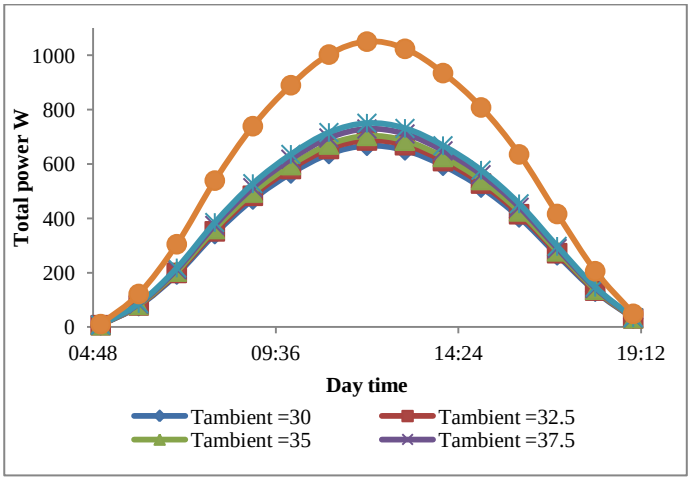

Fig. 8 The PV/T cells temperature and the effect of this temperature on the electrical efficiency

Fig. 9 The total power output from the PV/T for June month during the day. T ambient is in (^{0}C)

The effect of generator temperature on the COP of the absorption cycle at various condenser temperatures is shown in **Figure 11**. It clear that COP increases initially then a decrease occur as the generator temperature increase for various condenser temperature. There is an optimum generator temperature which depends on the value of the condenser temperature and this behavior is consistency with results reported by Kaushik and Arora, (2009). This can be explained by the fact that as the generator temperature increases the amount of refrigerant generated increases and this, in turn, leads to improve the COP. Although an increase in the generator temperature leads to an increase in the amount of refrigerant generated but an extra increase in generator temperature leads to an increase of the refrigerant temperature and thus reducing the COP. Also as shown when the condenser temperature increases the COP decreases this is due to the decrease of the heat rejected by the condenser.

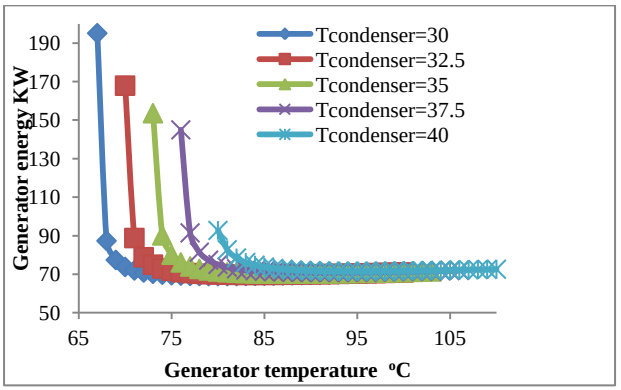

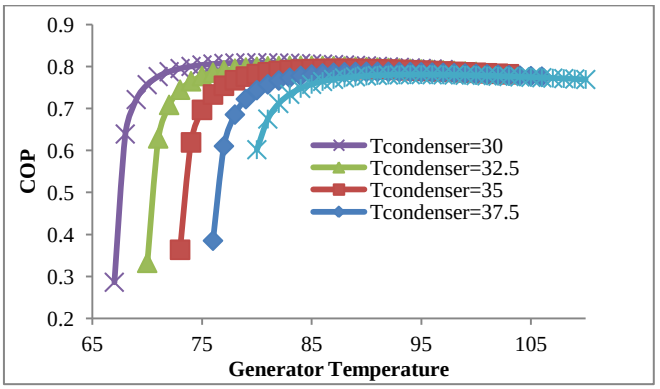

Fig. 10 The effect of generator temperature on the generator energy of the absorption cycle for various condenser temperatures (T ambient is in (^{0}C)).

Fig. 11 The effect of generator temperature on the COP of the absorption cycle for various condenser temperatures ($T_{ambient}$ is in (^{0}C))

Figure 12 represents the influence of the generator temperature on the water flow rate at various condenser temperature. It can be seen that as the generator temperature increases the needed water flow rate decreases, due to the increase of the amount of heat supplied by the water. In addition to the increase in the condenser, temperature leads to an increase in the water flow rate needed.

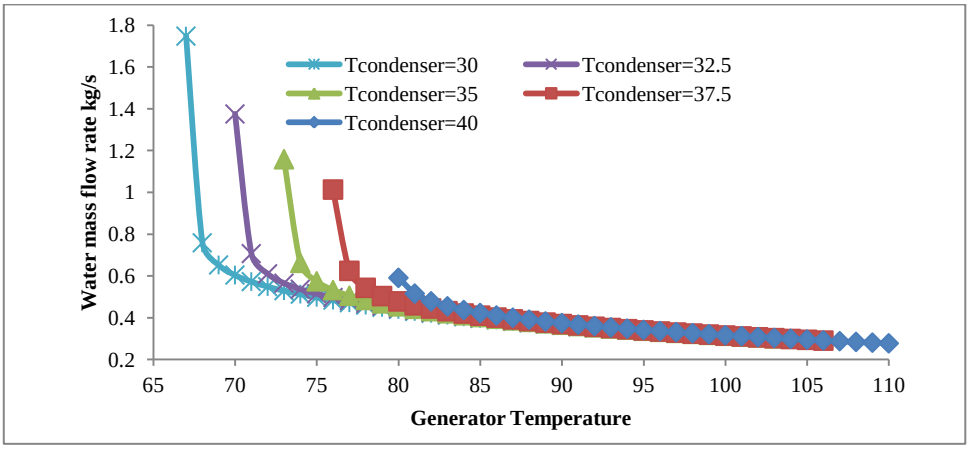

Fig. 12 The effect of generator temperature on the water flow rate of the absorption cycle for various condenser temperatures ($T_{ambient}$ is in (^{0}C)).

5. Case Study and Economical Analysis

The selected parameters that affect the performance of the cycle, are generator temperature, mass flow rate, and the number of collectors. Now to select the values of these parameters the conditions which the cycle runs on it should be known, to get the best performance and reduce the number of thermal photovoltaic modules to run this cycle. So if the system operated at an ambient temperature of 31° C, then the cycle should be operated at generator temperature Tg=80°C because if the system runs at this

generator temperature this will get the optimum performance of the cycle and will get the maximum COP of the cycle. Moreover at any other ambient temperature the system subjected to a slight decrease in the COP. At the optimum generator temperature, the PV/T collector generates about 170W electricity and 500W thermal power. The Average ambient conditions throughout the year in Irbid city is depicted in **Table 2.**

Table 2 Average ambient conditions throughout the year in Irbid city (Jordan Meteorological Department, 2016).

Month	1	2	3	4	5	6	7	8	9	10	11	12
Average max. temp. (°C)	2.9	4.1	6.9	2.1	6.9	9.9	1.1	1.3	9.8	6.6	0.6	5
Average min. temp .(°C)	.9	.4	.3	0.6	4.1	7.4	9.2	9.6	8.2	5.1	0.0	.4

5.1 Cost analysis

The cost analysis for the system at hand include the cost of the PV/T collectors and the cost of the absorption chiller. The economical investigation is presented in the following sections.

5.1.1 PV/T cost

The PV/T cost analysis was done by Tomas Matuska (2014) where the cost of the PV/T is 290 - 410 €/m^2 for nonselective type and 370 -500 €/m^2 for selective type PV/T solar collectors. In this research work, these values will be considered.

5.1.2 Absorption chiller cost

Absorption chiller cost was represented by the chiller cost, auxiliary cost, and maintenance cost this cost was correlated by Brown (2002) these correlations are represented in equations (22-24). The electricity for the absorption chiller and the condenser pumps, water pumps, and cooling tower fans will be supplied from the PV/T collector's electrical energy. The result of economic analysis as per the above assumptions are presented in **Table 3.**

Installed cost, \$=1,819.4 x $TR^{0.8452}$ (22)

Annual O&M = 20 x TR (23)

Auxiliary electricity consumption = 0.14KW/TR (24)

In summary, the system should be operated on a certain optimum parameters that yield the optimum performance. These optimum specific conditions are as follows: generator temperature TG=80 ^{o}C, evaporator temperature Te =7°C, and ambient temperature Tc = 32.5 °C. This condition can meet a cooling load of 16 TR. In addition, the COP value of the system was found to be equal to 0.81 which is considered a good value for the COP of the absorption refrigeration system. To supply the system by the heat required to drive the absorption refrigeration system at optimum conditions an area of 84 m^2 thermal photovoltaic collectors should be installed. Also, this system can be utilized for space heating due to a large amount of heat generated at higher efficiency

Conclusions

In this work, a mathematical model was developed for an absorption refrigeration cycle driven by a flat plat PV/T collector under Jordan climate conditions. The simulation study includes the thermal analysis, electrical analysis, and the absorption cycle performance. The results of this study show that the maximum solar radiation occurs in June and asymmetrical solar radiation in May and October. The thermal efficiency PV/T under the solar radiation range (500-1050) W/m^2 and wind speed 5 m/s the PV/T collector was found to be in the range of (63.9 -72.5 %). At constant solar radiation of 500 w/m^2 and a PV/T collector area of 1m^2

and a wind speed in that range of(1-12) m /s the thermal efficiency was computed to be in the range of (44.6 - 63.6 %). With wind speed of 5 m/s and solar radiation of 500W/m^2, 1m^2 of PV/T collector are and flow rate range (0.01-0.3) kg/s the thermal efficiency was found to be in the range of (63.9 - 68.3 %). The thermal efficiency remains constant after a flow rate equals 0.11 kg/s. The PV/T cells the efficiency decreases as the temperature as the ambient temperature increases.For the absorption refrigeration cycle as the condenser, temperature increases the minimum generator temperature needed to drive the cycle increases. At Jordan climate, the average maximum ambient temperature was found to be 31^{o}C so at this condition the maximum COP for the cycle was equal 0.81 and the generator temperature was 80^{o}C.

Nomenclature

A_c	=Collector area	[m^2]
b	=Bond width	[m]
C_b	=Bond conductance	[W/m^2 K]
COP	=Coefficient of performance	[-]
C_p	=Specific heat at constant pressure	[kJ/kg.^{o}C]
D_i	=Inner diameter of tube	[m]
D_o	=Outer diameter of tube	[m]
El	=Heat exchanger effectiveness	[-]
F	=Fin efficiency factor	[-]
F’	=Collector efficiency factor	[-]
FR	=Heat removal factor	[--]
G	=Solar radiation	[W/m^2]
hc,p_c	=Convective heat transfer coefficient from cover to ambient	[W/m^2. K]
hw	=Convective heat transfer coefficient from cover to ambient	[W/m^2. K]
hr,p_c	=Radiation heat transfer coefficient from plat to cover	[W/m^2. K]
hr,c_a	=Radiation heat transfer coefficient from cover to ambient	[W/m^2 K]
k	=Thermal conductivity	[W/m.K]
L	=Plate length	[m]
$\dot{m}$	=Mass flow rate	[kg/s]
Nu	=Nusselt Number	[-]
Q_u	=Useful thermal energy of PV/T	[W]
Q_e	=Evaporator energy	[W]
Q_g	=Generator energy	[W]
Pr	=Prandtle Number	[-]
Re	=Reynold Number	[-]
S	=Solar radiation	[W/m^2]
T_a	=Ambient temperature	[K)
T_i	=Inlet fluid temperature	[K]
T_o	=Outlet fluid temperature	[K]
T_{ab}	=Absorber temperature	[K]
T_{co}	=Condenser temperature	[K]
T_e	=Evaporator temperature	[K]
T_g	=Generator temperature	[K]
T_{pv}	=PV cells temperature	[^{o}C]
T_p	=Plat temperature	[K]
t	=Pipe thickness	[m]
U_l	=Overall heat loss coefficient	[W/m^2 K]
v	=Wind speed	[m/s]
Wp	=pump work	[W]
X	=Concentration	[-]
Greek Symbols		
β	=Cell efficiency temperature factor Emissivity	[-]
δ	=Fin thickness	[m]
ε	=Emissivity	[-]
η_o	=PV cell efficiency at standard conditions	[-]
η_{el}	=PV cells electrical efficiency	[-]
η_{th}	=PV/T thermal efficiency	[-]
μ	=Viscosity	[Pa.s]
ρ	=Density	[kg/m^3]
σ	=Stefan–Boltzmann constant	[W/m^2 K^4]

References

Ammar A., K. Sopian, M. Alghoul, B. Elhub, and Elbrek A., "Performance study on photovoltaic/thermal solar-assisted heat pump system", *Jour. of Therm. Analy. and Calor*. **136**, 79–87 (2019)

Assilzadeh F., S. A. Kalogirou, Y. Alia, and Sopianam K., “Simulation and optimization of a LiBr solar absorption cooling system with evacuated tube collectors”, *Renew. Energy,* **30**, 1143–1159 (2005)

Bhargava AK, Garg HP, and Agarwal R., “Study of a hybrid solar system-solar air heater combined with solar cells”, *ENERG CONVERS MANAGE*; **31**, 471–479 (1991)

Brinkworth B., Brinkworth and Sandberg M., “Design procedure for cooling ducts to minimize efficiency loss due to temperature rise in PV arrays”, *Sol.*

Energy, **80**, 89–103 (2006)

Brown D., Dirks J., "Economic Sizing and Dispatch of Central Energy Plant Equipment at the Navy Medical Center, San Diego", *Cogen.and Comp. Power J.*, **17,** 21-36 (2002)

Cengel Y., Ghajar A., "Heat and mass transfer fundamental and applications", 4th Edn., McGraw-Hill Higher Education, (2011).

Dai N., Xinyi X., Shuhong L., and Zheng Z. "Simulation of Hybrid Photovoltaic Solar Assisted Loop Heat Pipe/Heat Pump System", *Appl. Sci.*, **7**, 1-11 (2017)

Dubey S., and Tiwari G.,"Thermal modeling of a combined system of photovoltaic thermal (PV/T) solar water heater", *Sol. Energy*, **82**, 602–612 (2008)

Dubey S. and Subiantoro A., "Numerical Study of Integrated Solar Photovoltaic-Thermal Module with a Refrigeration System for Air-Conditioning and Hot Water Production under the Tropical Climate Conditions of Singapore", *Int J Air-Cond Refrig.*, **26**, 1850021-10 (2018)

Duffie J. A. and William A., "Solar Engineering of Thermal Processes", 4th Edn., John Wiley and Sons, Inc., (2013)

Fudholi A, Sopian K, Ruslan M., and Alghoul M., "Sulaiman MY "Review of solar dryers for agricultural and marine products", *Renew Sustain Energy Rev.*, **14**, 1–30 (2010)

Vokas G., N. Christandonis, and Skittides F., "Hybrid photovoltaic–thermal systems for domestic heating and cooling-A theoretical approach", *Sol. Energy*, **80**, 607-615 (2006)

Chamberlain G., "Organic solar cells: A review", *Sol Cells*, **8**, 47-83 (1983)

Gur M., Abraham K., Abraham D.,"Solar cooling with concentrating photovoltaic/thermal (CPVT) systems*", Energy and Management*, **47**, 3368-3382 (2007)

Ibrahim A., Mohd Y., Ruslan M., Sohif Mat, and Kamaruzzaman S.,"Recent advances in flat plate photovoltaic/thermal (PV/T) solar collectors", *RENEW SUST ENERG REV*, **15**, 352–365 (2011)

Jordan Meteorological Department (JMD), Solar data for Jordan (2011)

Kaushik S., Akhilesh A. "Energy and exergy analysis of single effect and series flow double effect water–lithium bromide absorption refrigeration systems", *INT J REFRIG.*, **32**, 1247–1258 (2009)

Kumar S., and Tiwari G., "An experimental study of hybrid photovoltaic thermal (PV/T)-active solar still", *Int J Energy Res.* **32**, 847–58 (2008)

Lasnier F and Ang T., Photovoltaic Engineering Handbook, Adam Higler (1990)

Leonardo M., Nabin S., Xichun L., Reddy K., Tapas K., "Opportunities and challenges in micro- and nano-technologies for concentrating photovoltaic cooling: A review", *Renew Sust Energ Rev*, **20**, 595–610 (2013)

Mario P., Rosaria C., and Giovanni P., "Flexible Solar Cells", *Chem Sus Chem*, **1**, 880–891 (2008)

Matuska T., "Performance and economic analysis of hybrid PVT collectors in solar DHW system", *Energy Procedia*, **48**, 150–156 (2014)

Mittelman G, Kribus A, Mouchtar O, and Dayan A., "Water desalination with concentrating photovoltaic/thermal (CPVT) systems", *Sol Energy***,83**, 1322–1334 (2009.

atlamwala T., Gadalla M., and Dincer I., "Performance assessment of an integrated PV/T and triple effect cooling system for hydrogen and cooling production", *Int J Hydrogen Energy.*, **36**, 11282–11291 (2011)

Srikhirin Pongsid ,Satha Aphornratan, Supachart Chungpaibulpatana, A review of absorption refrigeration technologies, *Renew Sust Energ Rev.*, **16**, 343–372 (2001)

Tintai C., Jie J., Hanfeng H., Gang P., Wei H., and Keliang L., "Distributed dynamic modelling and experimental study of PV evaporator in a PV/T solar-assisted heat pump", *Int. Jour. Heat Mass Trans.*, **52**, 1365–73 (2009

Tiwari G. Nayak S., Dubey S, Solanki S., and Singh R., "Performance analysis of a conventional PV/T mixed mode dryer under no load condition", *Int Jou. Energy Res.*, **33**, 919-930 (2009)

TWINSOLAR, http://www.grammer-solar.com/en/products/twinsolar/ index.shtml; 2010 (accessed 2012)

Tyagia V., Kaushika S., and Tyagib S., "Advancement in solar photovoltaic/thermal (PV/T) hybrid collector technology", *Renew Sust Energ Rev*, **16**, 1383–1398 (2012)

The Ceramic TiO2 Low-Pressure Nano-Filtration Membrane Separation Behavior for Single and Mixed Ion Salt Solutions

Banan Hudaib*[1], Rasha Hajarat[2], Zongwen Liu[3]

[1)]Al-Balqa Applied University, Faculty of Engineering Technology, Chemical Engineering Department, Amman 11131, Jordan
[2)]Mut'ah University, Department of Chemical Engineering, Al-Karak, Jordan
[3)]University of Sydney, School of Chemical and Biomolecular Engineering, NSW 2006, Australia

The objective of this work is to study the separation performance of a tubular TiO_2 ceramic nanofiltration membrane operate at low pressures (2 bar), and the parameters that would affect the membrane rejection behavior, such as the ions valences, ions type, transmembrane pressure (TMP) values, and membrane zeta-potential. The membrane was used to desalinate water samples containing NaCl, $NaNO_3$, and Na_2SO_4 in single and tertiary salts solution. The rejection of ions solutions took the following trend: R of sulphate (SO_4^{2-}) > R of nitrate (NO_3^{1-})>R of chloride (Cl^{1-})>*R* of sodium (Na^{1+}). The highest SO_4^{2-}rejection was about 62%, the highest NO_3^{1-} rejection was about 51%, the highest Cl^{1-} rejection was about 42%, and highest Na^{1+} rejection was about 37%.

Keywords: Low-pressure nanofiltration; Transmembrane pressure; Separation; Ceramic membrane

Introduction

Freshwater is very important for all aspects of life. Brackish water and seawater treatment considered a good solution as a source of fresh water. Among all the techniques used for desalination, pressure-driven membrane processes have a prominent position. Membranes processes have dominated the desalination market in recent times (Schäfer *et al*. 1998). Among their different types, nanofiltration membranes have become the most important advance in membranes technology for their advantages such as low operation pressure, high flux, high retention of multivalent ions and organic molecules and relatively low operation and maintenance cost (Lu *et al*., 2002).

Nanofiltration (NF) based process is widely used for desalting and purification as alternative separation techniques to the conventional salting-out processes (Morão *et al*., 2008) as one of the most recently developed membrane separation processes, (NF) has found some industrial applications such as pharmaceutical industry, drinking water treatment, and environmental protection (Bowen and Welfoot, 2002). Nanofiltration (NF) is operating under low pressures (less than 5 bar), potentially opening doors for scale-up implementation of the membrane in low-pressure hard water softening and seawater desalination pretreatment (Labban *et al.*, 2017). Ceramic NF membranes are regarded as the appropriate choice in many applications, due to their temperature stability, resistance towards solvents, narrow pore size distribution (Zhu *et al.*, 2018), several additives were used in the modification of mesoporous and microporous membranes include Al_2O_3, TiO_2, ZrO_2, SiO_2. Of these, TiO_2 has unique characteristics e.g higher chemical and physical stability, ability to withstand high temperatures; and importantly, long service-life (Bhave, 1991). Much research has been focused on the development of ceramic membranes with a TiO_2 NF. The membrane performance can be characterized by the retention of charged and uncharged solutes, as well as the solvent permeability (Schäfer *et al.* 1998, Mohammad & Takriff, 2003, Luo & Wan, 2013).

The separation process in nanofiltration is a combination of sieving and diffusion of molecules through the surface layer of the membrane. Also, surface charges play a more important role in the separation by NF than with other pressure-driven membrane processes (Manttari, 2006). The charge of nanofiltration membrane is a result of dissociating functional groups, adsorption of ions from the solution, adsorption of polyelectrolytes, adsorption of ionic surfactants, and adsorption of charged macromolecules (Luo, 2013, Yazhen & Lebrun, 1999). When the membrane is charged, then the Donnan effect would contribute to the separation performance. The charged membrane would repel ions with the same charge as the fixed membrane charge; as a result, the ion's concentration in the membrane and the transport rate are low (Luo, 2013, Mohammad & Takriff, 2003). Nanofiltration can separate charged and uncharged solutes from the solution, (Yazhen & Lebrun, 1999). The uncharged molecule's separation is a result of the size exclusion or the difference between the diffusion rates.

Received on February 4, 2019; accepted on August 27, 2019 Correspondence concerning this article should be addressed to Banan Ismail Hudaib (E-mail address: banan.hudaib@bau.edu.jo ORCiD ID of Banan Ismail Hudaib https://orcid.org/0000-0003-2900-6388

The charged solute's (ions) separation is a result of the interaction between the membrane surface charge and the solute charge. Also, charged molecules separation depends on their size; if the molecule size is bigger than the membrane pore, then it will be retained by the membrane (Luo and Wan, 2013, Yaroshchuk, 2000, Bargeman *et al.*, 2005). Solute permeates through nanofiltration membrane by two mechanisms: convection and diffusion. Convection transfer is affected by the physical parameters such as pressure and conversion rate, while diffusion transfer is affected by the chemical parameters such as concentration and pH. As a result, convection is more effective at high pressure than low pressure and larger ions are better retained by the membrane because convection depends on the physical parameters. Since diffusion depends on the chemical parameters, the chemical selectivity is more important than the physical selectivity in nanofiltration membrane; as a result, the selectivity is much higher at low pressure. Nanofiltration membrane selectivity is high at low pressure because of diffusion, and its retention is high at high pressure because of convection (Yaroshchuk, 2000; Szymczyk *et al.*, 2003). Another factor that affects NF membrane rejections is concentration polarization, which refers to the formation of concentration gradients on the membrane feed and permeates interfaces as different constituents of the feed solution permeates through the membrane at different rates. This change in concentrations at the membrane interfaces leads to a reduction in permeate flux and rejection ratios (Sablani *et al.*, 2001; Labban *et al.*, 2017). The retention in NF of different molecules in solution has been widely investigated (Lebbez *et al.*, 2002, Szoke *et al.*, 2003; Bargeman *et al.*, 2005). Bruggen *et al.* Studied the separation of mono- and divalent ions from aqueous solution by electrodialysis and nanofiltration in single solute systems (Van der Bruggen *et al.*, 2008). The pH effect on ion retentions was investigated by (Van Gestel *et al.*, 2002). Bodzek *et al.* investigate the application of both, the DS-5-DK NF membrane and the DS-3-SE RO membrane to softening of well and tap water. Their results revealed that NF, was more permeable than RO, and has sufficient selectivity and is more suited for softening applications (Bodzek *et al.*, 2002). Many researchers studied the developments in low-pressure polymeric NF softening membranes (Fang *et al.*, 2012,2015; Liu *et al.*, 2015).

The aim of this work is to investigate ceramic TiO_2 NF membrane permeation properties, efficiency and separation performance for single and multivalent ions at low pressure. The influence of surface charge (at certain pH) and its effect on the separation behavior of the membrane were investigated to obtain the best conditions to enhance the separation performance of nanofiltration membrane.

1.Materials and Methods

1.1 Materials

The salts used in the experiments were sodium chloride (NaCl), sodium nitrate ($NaNO_3$) and sodium sulfate (Na_2SO_4) with high purities as follows, $NaNO_3$≥99%, NaCl≥99.5%, Na_2SO_4≥99.99%. These salts were obtained from Sigma-Aldrich. The solution pH was controlled using sodium hydroxide (NaOH≥99.99%) and hydrochloric acid (HCl, 5.0M). NaOH was also used in the cleaning process of the membrane.

1.2 Experimental set-up

A tubular TiO_2 ceramic nanofiltration membrane (7.0 mm I.D, 10.0 mm O.D, 190 mm length and 0.9 mm mean pore radius, obtained from Inopor gmbh-Germany was used. The concentration of all salts used was 0.1 M. To study the separation behavior of the membrane; pure distilled water was used at first, and then distilled water with a single or tertiary salt solution was used. The bench-scale membrane rig is shown in **Figure 1**. The main components are a variable speed peristaltic pump (type 603S, Watson-Marlow, UK), magnetic stirrer (RW20, IKAMAG, UK), glass container, tubular membrane module, pressure-relief valve, PVC-reinforced flexible piping, neoprene flexible piping for the pump (Watson-Marlow, UK), flow-meter (Gemü Gebr Müller, Germany), pH/ORP controller (Oakton), Accumet pH/Ion/Conductivity meter (Fisher-Scientific, Model 50), balance and stopwatch.

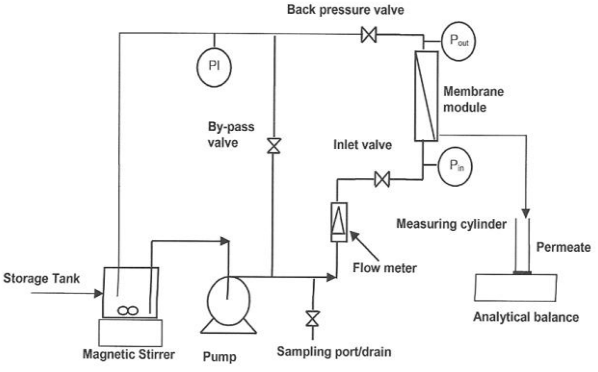

Fig. 1 Schematic diagram of the tubular NF membrane rig.

1.3 Experimental procedure

Initially distilled water was used to permeate through the ceramic membrane at constant inlet volumetric flow rate equal to 3.056×10-5 m^3/s (110 L/h), where the inlet pressure was increased from 0.3 bar to 2.0 bar, which gives transmembrane pressure (TMP) values between 0.2 bar to 1.9 bar, then single and tertiary salt solutions were used to compare the effect of ion type and ion charge on separation. At first sodium chloride (NaCl), sodium nitrate ($NaNO_3$) and sodium sulfate (Na_2SO_4) was prepared as a single solution with 0.1 M concentration. Then a mixed solution of the three salts was prepared at 0.1 M concentration for each salt. The pressure was

increased by 0.2 intervals every 30 minutes. The permeate was collected for 25 minutes. After each experiment the membrane was cleaned by washing with distilled water several times then it was cleaned with 0.1M NaOH solution for 1 hour, and finally, the membrane was washed with distilled water continuously for 6 hours. The anion's concentration was measured by using ion chromatography (Dionex DX600, Dionex AS4A-SC column) and ICP-AES was used to measure the cation concentration.

1.4 Membrane characterization

1.4.1 Membrane rejection

The rejection (R) of ion (i) using ceramic nanofiltration membrane is given as (Geraldes, 2008)

$$R = 1 - \frac{C_{i.p}}{C_{i.f}} \quad (1)$$

Where $C_{i,p}$ is the concentration of ion (i) in the permeate (mol/m) and $C_{i,f}$ is the concentration of ion (i) in the feed (mol/m).

The TMP was calculated as follows (Piry, 2008)

$$TMP = \left(\frac{P_{inlet} + P_{outlet}}{2}\right) - P_{permeate} \quad (2)$$

Where the pressure at the permeate side was assumed to be equal to zero, and hence the TMP would be as follows

$$TMP = \left(\frac{P_{inlet} + P_{outlet}}{2}\right) \quad (3)$$

1.4.2 Ceramic membrane structural morphology

Structural morphology of the used membrane was imaged by SEM (FEI Quanta 200, Purge, Czech Republic) and EDXS equipment (Amertek Inc, Paoli, PA, USA). The membrane-active and supporting layers are shown in **Figure 2** which shows a thicker skin layer, hence expected higher rejection and lower permeate flux (Chung *et al.*, 2005).

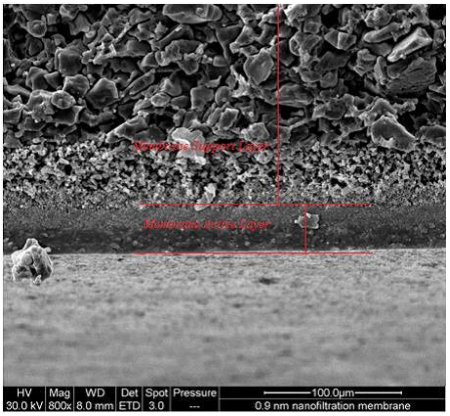

Fig.2 SEM image for ceramic nanofiltration membrane showed the active layer and support layer. Scale bar: 100 µm.

1.4.3 Zeta potential

The surface charge of the membrane surface was measured by using the electrophoretic mobility of TiO_2 membrane powder derived from the membrane top-layer. This method allows easy evaluation of the charge characteristics of the top-layer (Guizard *et al.*, 1999). The experiment was run at pH ranging from 3 to 10, at room temperature (25±0.50C). Sodium chloride (NaCl) salt 0.1M concentration was used. The pH of the solutions was titrated using 0.1M HCl, and 0.1M NaOH solutions. After preparing the solution, the crushed membrane was added to these solutions, and zeta potential was measured.

2 Results and Discussion

Studying Zeta potential is considered valuable to understand the interactions between the membrane surface and the solution in contact with the membrane as it has a significant effect on the membrane rejection. As shown in **Figure 3**, the results of zeta potential measurements stated that the membrane zeta potential decreased as the pH increased. Hence, the NF membrane has more negative charges and higher hydrophilicity with increasing pH (Manttari, 2006). The effective membrane, charge corresponds to the inherent charge due to protonation and dissociation of surface hydroxyl groups (Takagi, 2003). The pH used in all salts experiments was chosen to be 7 at which the zeta potential for the membrane found to be -20 mV. Single and tertiary salt solutions were used to compare the effect of ion type and ion charge on membrane separation. At first sodium chloride (NaCl), sodium nitrate ($NaNO_3$) and sodium sulfate (Na_2SO_4) was prepared as a single solution with 0.1 M concentration. Then a mixed solution of the three salts was prepared at 0.1M concentration for each salt. For ($NaNO_3$) solution, results showed that the rejection of nitrate ions NO_3^{1-} was slightly higher than the rejection of sodium ions Na^{1+} see **Figure 4**. The rejections of cations and anions were negative (except at the

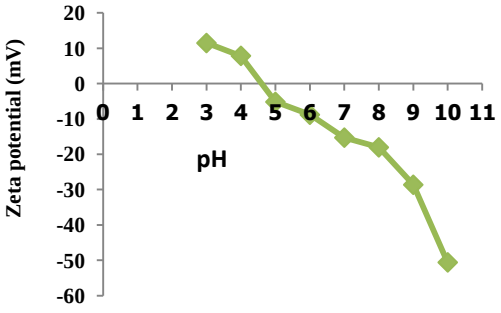

Fig. 3. Zeta potential at 0.1M concentration

lowest TMP value,

0.2 bar) same results were reported by Yaroshchuk (Yaroshchuk, 2008). This means that the electrostatic interaction between the membrane and ion charges was not strong enough to overcome the effect of TMP on rejection. Thus, negative rejection does not mean that mass (Na^{1+} solute is this case) is being created, neither the mixture now has more Na^{1+} ions than it initially started with. Negative rejection only implies that the system has a higher concentration of Na^{1+} in the permeate, relative to the feed. In other words, negative rejection for a given ion species only occurs when more of that ion is in the smaller permeate volume relative to the much larger feed volume. (Yaroshchuk, 2008; Labban *et al.*, 2017).The higher rejection for both ions was at the lowest TMP at 0.2 bar, the rejection of NO_3^{1-} was about (63%) slightly higher than the rejection of Na^{1+} about (53%). Since both ions have the same charge strength, the electrostatic interaction with the membrane charge would be at the same magnitude, and due to neutrality condition at both sides of the membrane, the anion rejection was higher for the ion with bigger size as the size plays an important role in the rejection of NO_3^{1-} (Pontalier *et al.*, 1997; Nystrom *et al.*, 1995). Additionally, the NO_3^{1-} ion charge plays a role in the rejection as it has the same membrane charge, which caused its repulsion away from the membrane, thus enhancing its rejection (Nystr¨om *et al.*,1995; Garcia *et al.*, 2006). While for Na^{1+}, its charge is opposite to membrane charge, leading to increasing its permeation through the membrane, the rejection of cation Na^{1+} had negative rejection values. Since negative rejection values which imply that the system has a higher concentration of a given ion in the permeate, relative to the feed (Yaroshchuk *et al.*, 2008; Labban *et al.*, 2017). In general, it can be noticed that the rejection of NO_3^{1-} remained almost constant as the TMP increased, while the rejection of Na^{1+} slightly increased as the TMP increased.

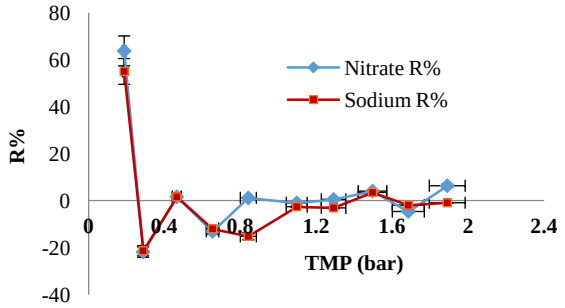

Fig. 4 Sodium nitrate rejection versus TMP at pH=7. The error bars are based on 10% error in measuring the permeate concentration

For Na_2SO_4 solution permeate, flux increased from $2.8x10^{-8}$ to $5.0x10^{-7}$ $m^3/m^2/s$ as the TMP increased. Results found that (SO_4^{2-}) ions rejection was higher than the rejection of (Na^{1+}) ion, see Figure 5. This may be attributed to Donnan exclusion and ion size effect. The electrostatic interaction (Donnan exclusion) between the membrane charge (which is negative) and SO_4^{2-} charge. The high negative valence of SO_4^{2-}, causes more repulsion between the negative membrane and SO_4^{2-} charges, which results in more rejection of SO_4^{2-} ion (Garcia *et al.*, 2006; Teixeira *et al.*, 2005, Luo & Wan, 2013), Similar results were also reported by Szoke *et al.* (Szoke *et al.*, 2003) for single $Na_2SO_4^{2-}$ and $CaCl_2$ solutions. On the other hand, the cation Na^{1+} is attracted by the membrane charge and passes freely through the membrane as shown in the results seen in **Figure 5**. Hence, the rejection of cation Na^{1+} had some negative rejection values (Yaroshchuk *et al.*, 2008; Labban *et al.*, 2017; Gilron *et al.*, 2001).

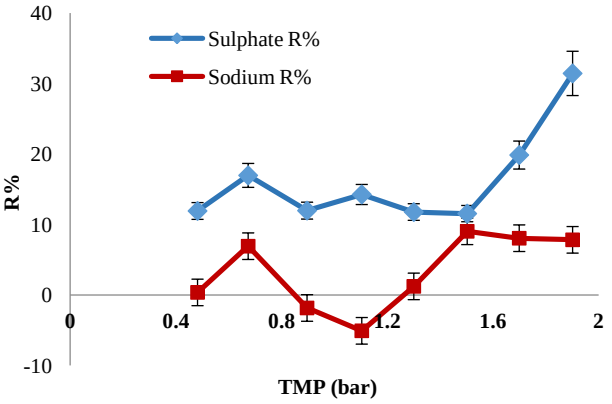

Fig. 5 Sodium sulfate rejection versus TMP at pH=7, The error bars are based on a 10% error in measuring the permeate concentration.

For NaCl solution, results showed that the rejection of chloride (Cl^{1-}) ions was higher than the rejection of sodium (Na1+) ions see **Figure 6**. The rejection of Cl^{1-} ions increased as the TMP increased; This may be due to electrostatic interaction between the membrane charge (which is negative in this case) and the ion charge. Hence, the rejection of Cl^{1-} is a result of the repulsion between the negative membrane and Cl^{1-} charges (Pontalier *et al.*,1997, Luo & Wan, 2013), this together with Cl^{1-} ion size made its rejection higher than Na1+ rejection, same results was mentioned by Luo *et al.* (2013) and Teixeira *et al.* (2005). The electro-neutrality condition can explain the low rejection of both ions at both sides of the membrane. Where Cl^{1-} and Na1+ had to diffuse through the membrane to neutralize the charge on the permeate side. See Fig. 6. The highest rejection of Cl^{1-} was about 22% at a TMP value equal to 1.9 bar. On the other hand, the Na^{1+} rejection increased as TMP increased until it reached 1.5 bar where it decreased afterward. The highest rejection of

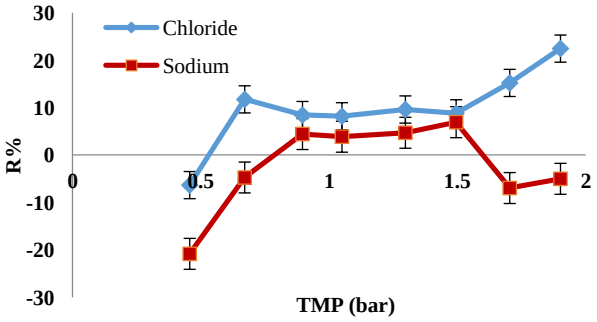

Fig. 6 Sodium chloride rejection versus TMP at pH=7. The error bars are based on 10% error in measuring the permeate concentration

Na^{1+} was about 8% at a TMP value equal to 1.5 bar.The mixed salt solution permeates flux increased from 4.7×10^{-9} to 5.0×10^{-7} $m^3/m^2/s$ as the TMP increased. As seen in **Figure 7**, the rejection of ions took the following trend: *R* of sulfate (SO_4^{2-})> R of nitrate (NO_3^{1-})>*R* of chloride (Cl^{1-})>*R* of sodium (Na^{1+}). The rejection of all anions decreased with the initial TMP and remained almost constant as the TMP increased. The highest rejection for all anions was at the lowest TMP. The highest SO_4^{2-} rejection was about 62%, the highest NO_3^{1-} rejection was about 51%, and the highest Cl^{1-} rejection was about 42%. The rejection of cation Na^{1+} decreased after the initial TMP and almost stayed constant as the TMP increased. The highest Na^{1+} rejection was about 37%. In general, cation Na^{1+} had negative rejection values, which means that it passed freely through the membrane as explained before (Yaroshchuk *et al.*, 2008; Labban *et al.*, 2017; Gilron *et al.*, 2001). The rejection of ions can be explained by the Donnan exclusion, electro-neutrality condition at both sides of the membrane and ion size. Since the anions had the same charge as the membrane, this would cause repulsion of the anions away from the membrane and back to the solution. Since the cation Na^{1+} had an opposite charge to the membrane charge, this caused the cation to pass through the membrane and decrease its rejection rate. The ion size influenced rejection where rejection increased as the ion size increased; Furthermore, electro-neutrality played an important role in the rejection of ions (Pontalier *et al.*, 1997; Luo & Ding, 2011). To maintain the electro-neutrality condition at both sides of the membrane, ions had to pass through the membrane, which explains the low rejection values for both the cation and the forming HSO_4^{1-}. As a result, more Na^{1+} has to pass through the membrane to maintain the electro-neutrality condition, and this explains the low rejection of Na^{1+} ion. For higher TMP values, the mentioned conditions above would be considered negligible when comparing them to the pressure force. This might explain the decrease in rejection rate as the TMP increased. Moreover, since it is the main driving force, this would explain why the ion rejections remained constant as the TMP increased. When comparing the separation of ions from a single salt solution and mixed salt solution, it was noticed that the rejection of cation Na^{1+} from single salt solution or mixed salt solution did not differ. This means that Na^{1+} was not affected by the anion type or concentration of cation or anions. The same was noticed for SO_4^{2-} and Cl^{1-} anions, where their rejections from the single salt solution and mixed salt solution were almost similar. This means that their rejections were not affected by the existence of other types of anions. On the other hand, this did not imply for NO_3^{1-} anion, where its rejection from mixed salt solution was higher than its rejection from the single salt solution.

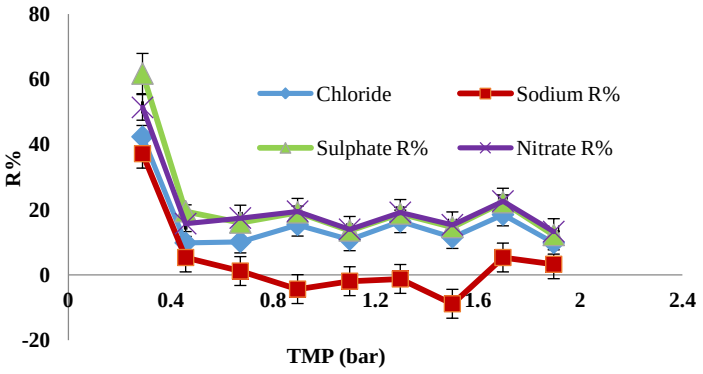

Fig. 7 Mixed salt rejection versus TMP at pH=7. The error bars are based on 10% error in measuring the permeate concentration

Conclusions

The present study has investigated the separation behavior of ceramic NF membrane under low-pressure for single and tertiary combinations of mixed salts solutions containing sodium chloride (NaCl), sodium nitrate ($NaNO_3$), and sodium sulfate (Na_2SO_4). It was found that the trend of rejection of ions as the following: R of sulphate (SO_4^{2-}) > R of nitrate (NO_3^{1-}) > R of chloride (Cl^{1-}) > R of sodium (Na^{1+}). The rejection of the common Na^{1+} cation from single and mixed salt solutions by 0.9 nm ceramic TiO_2 nanofiltration membrane was found to be independent of the anion type where Na1+ cation had the lowest rejection from single salt and mixed salts solutions. The rejections of SO_4^{2-} and Cl^{1-} anions from single and mixed salts solutions were found to be independent of the anion type. The rejection of the NO_3^{1-} anion from the mixed salt solution, was found to be higher than from a single salt solution. Except at the lowest TMP was the rejection of the NO_3^{1-} anion from the mixed salt solution was found to be lower than from a single salt solution.

Nomenclature

$C_{i,p}$	=Concentration of ion i in permeate	[mol/m^3]
$C_{i,f}$	=Concentration of ion i in feed	[mol/m^3]
M	=Molarity	[mol/L]
NF	=Nanofiltration membrane	[-]
$P_{permeate}$	=Pressure at the permeate side	[bar]
R	=Rejection of ion	[%]
TMP	=Transmembrane pressure	[bar]

References

Abdul-Wahab M., Sobri T., "Predicting flux and rejection of multicomponent salts mixture in nanofiltration membranes", *Desal*., **157**, 105-111 (2003).

Baldeón T., "Studies of electrically enhanced membrane processes", Thesis, Department of Chemical Engineering, The University of Manchester Institute of Science and Technology (2002).

Bargeman, G., Vollenbroek J., Straatsma J. Schroen C., and Boom R., "Nanofiltration of multi-component feeds, Interactions between neutral and charged components and their effect on retention", *J. Membr. Sci*., **247**, 11-20 (2005).

Bhave, R., "Inorganic Membranes Synthesis, Characteristics and Applications",1st Ed., Van Nostrand Reinhold, New York (1991).

Bodzek, M., Koter S., and Wesołowska K., "Application of membrane techniques in a water softening process", *Desal.*, **145**,1-3, 321-327 (2002).

Bowen, V.,. and Welfoot J., "Predictive modeling of nanofiltration: membrane specification and the process of optimization", *Desal.*, **147**, 197-203 (2002).

Cavaco M., A., Szymczyk A., Fievet P., and Brites A., "Modelling the separation by nanofiltration of a multi-ionic solution relevant to an industrial process", *J. of Memb. Sci.*, **322**, 320-330 (2008).

Childress, A., and Menachem E., "Effect of solution chemistry on the surface charge of polymeric reverse osmosis and nanofiltration membranes", *J. of Memb. Sci*, **119**, 253-268 (1996).

Chung, C., Quoc, N., and Hoai, N., "Influence of surface charge and solution pH on the performance characteristics of a nanofiltration membrane Influence of surface charge and solution pH on the performance characteristics of a nanofiltration membrane", *Sci. and Tech. of Adv. Mater*., **6** , 246-250 (2005).

Fang, W., Shi L., and Wang R., "Interfacially polymerized composite nanofiltration hollow fiber membranes for low-pressure water softening", *J. of Memb. Sci*, **430**, 129-139 (2013).

Fang, W., Shi L., and Wang R., "Mixed polyamide-based composite nanofiltration hollow fiber membranes with improved low-pressure water softening capability", *J. of Memb. Sci*, **468,** 52-61 (2014).

Garcia, F., Ciceron D., Saboni A., and Alexandrova S., "Nitrate ions elimination from drinking water by nanofiltration: Membrane choice", *Sep. and Purif. Tech.*, **52**, 196-200 (2006).

Geraldes, V., de Pinho, M., Fonseca, C., and Duarte, E., "Spiral-Wound Module Nanofiltration of Surface River Water", *E-Water* Hennef, Germany, 1-13 (2008).

Gilron, J., and Kedem O., "Experimental analysis of negative salt rejection in NF membranes", *J. of Memb. Sci*., **185**, 223-236 (2001).

Guizard, C., Palmeri J., Amblard P., Diaz J., and Lasserre J., "Basic transport phenomena of aqueous electrolytes in sol-gel derived meso and microporous ceramic oxide membranes", *Proceedings of the Ninth CIMTEC of World Ceramic Congress on Application to Commercial Ceramic Nanofilter Performance*, Florence, Italy, 14-19 June, 202-205 (1999).

Labban O., Chang L., Tzyy H., John H., and Lienhard V., "Fundamentals of Low-Pressure Nanofiltration: Membrane Characterization, Modeling, and Understanding the Multi-Ionic Interactions in Water Softening", *J. of Memb. Sci*, **521**, 18-32 (2017).

Labbez C., Fievet P., Szymczyk A., Vidonne A., Foissy A., and Pagetti J., "Analysis of the salt retention of a titania membrane using the DSPM model: effect of pH, salt concentration and nature", *J. of Memb. Sci*, **208**, 315-329 (2002).

Lu X., X., and Shi L., "Preparation and characterization of NF membrane", *J. of Memb. Sci*., **201**, 1-9 (2002).

Liu C., Shi L., and Wang R., "Crosslinked layer-by-layer polyelectrolyte nanofiltration hollow fiber membrane for low-pressure water softening with the presence of SO4 in feed water", *J. of Memb. Sci*, **486**, 169-176 (2015).

Luo, J. and Ding L., "Influence of pH on treatment of dairy wastewater by nanofiltration using shear-enhanced filtration system", *Desal*., **278**, 150-156 (2011).

Luo, J. and Wan Y., "Effects of pH and salt on nano-filtration - a critical review", *J. Membr. Sci.*, **438**, 18-28 (2013).

Manttari, M., Pihlajamaki A., and Nystrom M., "Effect of pH on hydrophilicity and charge and their effect on the filtration efficiency of NF membranes at different pH", *J. Membr. Sci.*, **280**, 311-320 (2006).

Nyström, M., Kaipia L., and Luque S., "Fouling and retention of nanofiltration membranes", *J. Membr. Sci*., **98**, 249-262 (1995).

Pontalier, P., Ismail, A. and Ghoul, M "Mechanisms for the selective rejection of solutes in nanofiltration membranes", *Sep. and Purif. Tech.*, **12**, 175-181 (1997).

Piry, A., Kühnl W., Grein T., Tolkach A., Ripperger S., and Kulozik U., "Length dependency of flux and protein permeation in crossflow microfiltration of skimmed milk",*J. Membr. Sci.*, **325**, 887-894 (2008).

Sablani, S., Goosen M., Al-Belushi R., and Wilf M., "Concentration polarization in ultrafiltration and reverse osmosis: a critical review", *Desal.*, **141**, 269-289 (2001).

Schäfer, A., Fane A., and Waite T., "Nanofiltration of natural organic matter: Removal, fouling and the influence of multivalent ions", *Desal.*, **118**, 109-122 (1998).

Schäfer, A., Fane A., and Waite T., "Nanofiltration principles and applications", 1st Ed., Elsevier, (2005).

Szoke, S., Patzay G., and Weiser L., " Characteristics of thin-film nanofiltration membranes at various pH-values", *Desal*., **151**, 123-129 (2003).

Szymczyk, A., Labbez C., Fievet P., Vidonne A., Foissy A., and Pagetti J., "Contribution of convection, diffusion and migration to electrolyte transport through nanofiltration membranes", *Adv. in Coll. and Inter. Sci.*, **103**, 77-94 (2003).

Takagi, R., Larbot A., Cot L., and Nakagi M., "Effect of Al2O3 support en electric properties of TiO2/ Al2O3 membrane formed by sol-gel method", *J. of Memb. Sci*, **177**, 33-40 (2000).

Teixeira, M., Rosa M., and Nyström M., "The role of membrane charge on nanofiltration performance*", J. Membr. Sci*., **265**, 160-166 (2005).

Van der Bruggen, B., Manttari M., and Nyström M., "Drawbacks of applying nanofiltration and how to avoid them: a review", *Sep. Purif. Tech*.., **63**, 251-263(2008).

Van Gestel, T., Vandecasteele C., Buekenhoudt A., Dotremont C., Luyten J., Leysen R., Van der Bruggen B., and Maes G., "Salt retention in nanofiltration with multilayer ceramic TiO2 membranes", *J. Membr. Sci.*, **209**, 379-389 (2002).

Wang, X., Zhang C., and Ouyang P., "The possibility of separating saccharides from a NaCl solution by using nanofiltration in diafiltration mode*", J. Membr. Sci*., **204**, 271-281 (2002).

Yaroshchuk, A., "Asymptotic behaviour in the pressure-driven separations of ions of different mobilities in charged porous membranes", *J. of Memb. Sci*, **167**, 163-185 (2000).

Yaroshchuk, A., "Negative rejection of ions in pressure-driven membrane processes", *Adv. in Coll. and Inter. Sci.*, **139**, 150-173 (2008).

Yazhen, X., and Rémi E., "Comparison of nanofiltration properties of two membranes using electrolyte and non-electrolyte solutes", *Desal.*, **122**, 95-106 (1999).

Yazhen, X., and Rémi E.,"Investigation of the solute separation by charged nanofiltration membrane: effect of pH, ionic strength and solute type", *J. of Memb. Sci*, 158, 93-104 (1999).

Zhu, B., Duke, M., Dumée, L., Merenda, A., des Ligneris, E., Kong, L., and Gray, S. "Short review on porous metal membranes-Fabrication, commercial products, and applications", *Membr.*, **8**, 1-27 (2018).

Adsorption of Malachite Green by Jordanian Diatomite Ores: Equilibrium Study

Emad El Qada
Chemical Engineering Department, Mu'tah University, Karak, Jordan

The focal theme of this work is to assess the ability of Jordanian diatomite to treat MG-bearing effluents. Effects of several experimental parameters namely, particle size of diatomite, pH and initial MG concentration were investigated through liquid-phase adsorption processes. Several equilibrium isotherm models were applied. It was found that initial MG concentration, pH and particle size of diatomite had a significant effect on the adsorption process. MG uptake has increased from 99.3 mg/dm^3 to 898.7 mg/dm^3 over the whole concentration range. A high percentage of MG removal (99.6%) was achieved as the diatomite particle size decreased from 500-710µm to 125-250µm. The optimum pH for the removal of MG was=9. Freundlich model was satisfactorily applied to the experimental data.

Keywords: Adsorption, Equilibrium isotherm, Malachite green, Diatomite, Wastewater Treatment**.**

Introduction

Malachite green (MG) is a cationic triphenylmethane dye that forms positively charged colored molecules when dissolved in water (Litefti *et al.*, 2017). Many industries, including textile, cotton, pulp, leather, food and wool, are using MG for coloring (Al-Wahbi, 2018). It is also used as an antifungal, antiseptic and antiprotozoan agent in aquacultures and animal husbandry (Oktay *et al.*, 2016; Heydaria and Khavarpour, 2018). Thus, such industries are considered as a major source of MG dye in water bodies (Lee *et al.*, 2018). Today MG is receiving much more attention due to its adverse effects on human beings as well as on aquatic ecosystems. Several researchers have reported several health hazards associated with the use of MG (Yang *et al.*, 2017; Pan and Zhang, 2009; Roja *et al.*, 2017). However, MG is still detected in foodstuff, fish and animal milk, due to illegal use (Pan and Zhang, 2009). MG is recognized as a stable dye with low biodegradability which makes the natural decolorization of its effluents a difficult process. Thus, the discharges of MG-bearing effluents into the water bodies represent a serious threat to aquatic life. Hence, treatment of such effluents before its final disposal to the aquatic environment is very important (Litefti *et al.*, 2017). Several technologies classified as chemical, biological and physical processes have been assessed for the remediation of wastewater contaminated with dyes such as flotation, ozonation, filtration, chemical oxidation, coagulation, aerobic and anaerobic microbial degradation, etc. However, none of these conventional methods has the necessities required for the successful treatment process: high efficiency and low capital cost (Lee *et al.*, 2018). Ali *et al.* (2018) asserted that most of the remediation technologies currently available are expensive and non-ecofriendly. Chowdhury and Saha (2013) announced that these methods pose techno-economical limitations for field-scale applications. In addition, the complex chemical structure of dyes enables them to resist fading with time and on exposure to sunlight, water, soap and many chemicals. Therefore, conventional wastewater treatment processes may not be the suitable choice for treating dyes effluents (Oktay *et al.*, 2016). One of the most economical, attractive, reliable and effective decolourization process is adsorption (Oktay *et al.*, 2016). It is not only a promising physicochemical technique for removing colour from wastewater, but it also offers the best potential for a wide range of pollutants removal. Moreover, it shows superiority comparing to the other treatment processes because of its low initial cost, sludge-free operation, simplicity of design, ease of operation, recovery of the sorbate, insensitivity to toxic substances, low energy demand and high quality of the treated effluent (Oktay *et al.*, 2016; Heydaria and Khavarpour, 2018; Ali *et al.*, 2018). Since the efficiency of the adsorption technology mainly depends on the cost and removal capacity of adsorbents used (Litefti *et al.*, 2017), it is of crucial important to seek for an eminent material to be used in the adsorption process. Many investigators have focused on innovation of low cost, commercially abundant and eco-friendly adsorbent with superior adsorption capacity. Currently, diverse attractive natural adsorbents have been examined for their efficient use as adsorbents for removing dyes from wastewater such as bentonite (Blanco-Flores *et al.*, 2016), wood apple shell (Sartape *et al.*, 2017), algal biomass (Gajare and Menghani, 2012), Chinese diatomite (Tian *et al.*, 2016), and clay (Dhahir *et al.*, 2013).

Received on September 2, 2019; accepted on November 16, 2019 Correspondence concerning this article should be addressed to Emad. El Qada (E-mail address: e_anadele@yahoo.com ORCiD ID of Emad El Qada https https://orcid.org/0000-0002-3364-8618.

Diatomite earth also known as diatomite is a soft, lightweight and pale naturally occurring sedimentary rock made up of diatoms. The main component of diatomite is micro-amorphous silica (SiO_2. nH_2O) (Alali, 2015; Salman *et al.*, 2016). It is available in abundance in different locations worldwide including the Middle East. Jordan has a substantial source of diatomite (150 Km^2) where it is located in the Azraq area; 110 km away from Amman. Jordanian diatomite consists mainly of 41-70.7% SiO_2, 10-16% Al_2O_3, 2.35-9.9 % Fe_2O_3, 2-4% Na_2O, 1-2% K_2O and traces of MgO, TiO_2, MnO and P_2O_5 (Alali, 2015). Different unique and outstanding physicochemical characteristics, such as high surface area, good absorptive capacity, high porosity, chemical inertness, and low density, make diatomite a valuable material and enable it to play an important role in the adsorption process (Alali, 2015; Salman *et al.*, 2016). The existence of an active silanol group distributed over the silica surface which can react with several organic compounds is another advantage for the adsorption process (Khraisheha *et al.*, 2005). Numerous researches showed that diatomite is gaining ground in the adsorption process due to its remarkable efficiency in removing a wide range of pollutants (Salman *et al.*, 2016; Khraisheha *et al.*, 2005; Erdem *et al.*, 2005; Alkan *et al.*; 2018). The use of Jordanian diatomite for the removal of MG from aqueous solution has not been reported in the literature. Therefore, this paper involves an equilibrium study is part of on-going research that is directed to study the feasibility of using the Jordanian diatomite for the removal of MG dye from textile wastewaters.

1 Materials and Methods

1.1 Adsorbate

Basic dye namely malachite green (purity = 99%) supplied by ACROS organics, USA, was chosen as principal adsorbate and was used without further purification. The chemical formula of MG is $C_{23}H_{25}N_2Cl$ (molecular weight=364.92 g/mol). **Figure 1** depicts the molecular structure of MG.

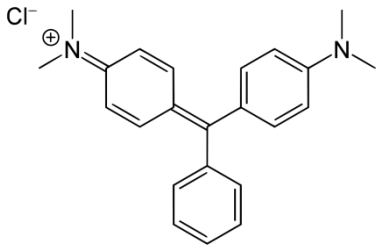

Fig. 1 Molecular structure of malachite green

1.2 Solvent

Deionized water (18.2 μΩ) was the preferred solvent in this work and was used to prepare both the stock MG solutions and reagents**.**

1.3 Adsorbent

Due to the superior physicochemical characteristics of diatomite, Jordanian diatomite (surface area = 56.23 m^2/g) was chosen as a potential adsorbent for removing MG from aqueous solution. Diatomite was supplied by the Natural Resources Authority, Amman, Jordan. First, diatomite was washed repeatedly with deionized water to eliminate any impurities, dried at 105^oC overnight under inert condition and desiccated to remove any remaining moisture. Then, it was crushed and sieved to the desired particle sizes. No chemical treatments were applied to the diatomite prior to the batch experiments. Detailed information about the characterization of Jordanian diatomite has been reported elsewhere (Khraisheha *et al.*, 2005; Shawabkeha and Tutunji, 2003; Al-Degs *et al.*, 2000).

1.4 Equilibrium Adsorption

A series of batch adsorption experiments have been undertaken to investigate the adsorption efficiency of MG onto Jordanian diatomite under different experimental conditions: pH, initial MG concentration and adsorbent particle size. All other factors are kept constant while carrying out the experiments. An accurately weighed quantity of adsorbent (0.025g) of a pre-determined size of diatomite (500-710μm) was added into eight glass sample jars. Stock of MG solution was prepared (1000 ppm) and further diluted accordingly to obtain the desired concentrations within the range 100-900 ppm. A 25 ml $\pm$ 0.5 ml of the MG solution of specific concentration were then added to the glass sample jars. The pH of MG solutions was adjusted to the desired value using 0.1M HCl/NaOH solution. Each jar was sealed using parafilm and screwing the top lids. The jars were then placed in a mechanical shaker at 200 rpm for the pre-determined period to reach equilibrium (1 week). Upon equilibrium the jars were removed from the shaker, and samples of 4-5ml $\pm$ 0.5 ml were withdrawn and filtered through 0.45 μm cellulose nitrate membrane - after passing enough volume of the dye solution through the filter paper to make sure that no dye is lost and absorbed by the filter paper-, diluted and analysed using Varian Cary-50 UV/VIS spectrophotometer (USA) at λ_{max} = 617 nm. Predetermined standard calibration curves for MG at each pH were used to measure the residual MG concentration. For particle size and initial MG concentration effects, three different sizes of various meshes (125-250μm, 250-500μm and 500-710μm) and different initial concentrations (100-900 ppm) were prepared and used. Other parameters like pH, mass of adsorbent and temperature were kept constant. All isotherm adsorption experiments were done in duplicate at room temperature and the mean values were used, as the accepted

value, in analyzing the data. The removal efficiency of MG and the amount of MG uptake at equilibrium (q_e, mg/g) was calculated using Eq. (1) and Eq. (2), respectively:

$$\text{Dye removal efficiency } (\%) = \frac{C_o - C_e}{C_o} * 100 \quad (1)$$

where C_o and C_e are the initial and equilibrium dye concentration (mg/dm^3), respectively, and:

$$q_e = \frac{(C_o - C_e)V}{m} \quad (2)$$

where q_e is the amount of MG adsorbed at equilibrium (mg/g); m is the mass of the diatomite (g) and V is the volume of MG solution (dm^3).

2 Results and Discussion

2.1 Adsorption Equilibrium

Designing any adsorption system is highly depends on adsorption isotherm. Adsorption isotherm is a valuable tool usually used to describe interaction and equilibrium relationships between adsorbent and adsorbate and by which the adsorption capacity of the adsorbent is established (Heydaria and Khavarpour, 2018; Lee *et al.*, 2018). The determination of adsorption isotherm is the first step in evaluating adsorbent performance toward adsorbate (Al-Degs, 2000). Different experimental factors such as pH, initial dye concentration, dose of adsorbent, particle size of adsorbent, contact time and temperature are believed to have great influences on the adsorption efficiency. In this respect, pH, initial concentration of MG solution and diatomite particle size were adopted as possible candidates influencing the adsorption process in this study.

2.1.1 Effect of Initial Concentration

The initial concentration of adsorbate solution plays a fundamental role in the adsorption process. A set of experiments were carried out to study the effect of initial MG on the adsorption process. Different initial MG concentrations (100, 300, 500, 700 and 900 mg/dm^3) were used. **Figure 2** shows the effect of initial MG concentration on the amount of MG adsorbed and on the removal efficiency. The figure reveals that MG uptake has increased with the increase in initial MG concentration. Approximately 88% increase in MG uptake was observed under the optimum conditions. Increasing initial MG concentration has increased the concentration gradient (driving force) between MG solution and diatomite surface, thus, enhancing MG uptake, which agrees with previously reported results (Pragathiswaran *et al.*, 2016). It is clear that a reduction in the removal efficiency (13%) has occurred as the initial MG concentration increased from 100-900 (mg/dm^3). This is due to the high competition between MG molecules for the fixed number of available adsorption sites on diatomite surface in the case of higher initial concentration (Heydaria and Khavarpour, 2018). This availability is reduced with the increase in initial MG concentration as most of the adsorption sites became saturated, thus, the removal efficiency was reduced. Therefore, the adsorption process is highly affected by initial MG concentration.

2.1.2 Effect of pH:

To ascertain the effect of pH on the adsorption of MG onto Jordanian diatomite, MG solution was conditioned to different pH values covering acidic and alkaline range (3–9). **Figure 3** shows the adsorption capacity of MG as a relationship between the amount of MG uptake at equilibrium, q_e, and its final concentration in the aqueous solution, C_e, at different pH values between 3 and 9. As seen from the figure, increasing the solution pH increases the adsorption capacity of MG onto the Jordanian diatomite. The maximum adsorption capacity attained was 541.1, 705.5, 730.2 and 816.2 (mg/g) for pH values of 3, 5,7and 9, respectively. MG as a cationic dye occurs in the aqueous solution in the form of positively charged ions. Thus, its adsorption onto the adsorbent surface will be governed by the adsorbent surface charge which in turn is affected by the pH of the solution (Lee *et al.*, 2018). Hence, by

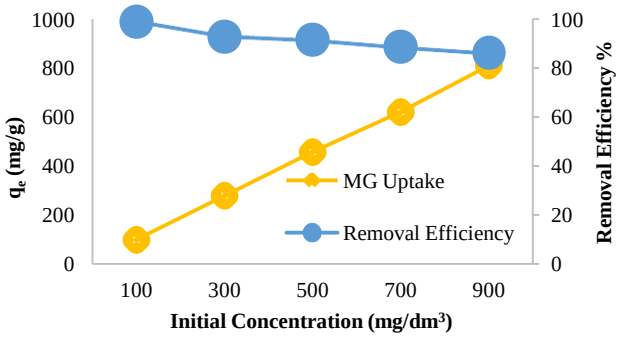

Fig. 2 Effect of the initial dye concentration on the adsorption of MG onto diatomite. Volume of dye solution=25 mL, mass of adsorbent=0.025 g, pH=7, particle size=250-500µm, temperature =25°C.

increasing the solution pH, the number of hydroxyl groups, as well as the number of negatively charged sites on the diatomite surface, will be increased and this favors the attraction between MG and diatomite surface (Lai and Chen, 2001). Consequently, Jordanian diatomite operates well in alkali conditions. These results agree well with previously reported results (Ren *et al.*, 2016). The reason for the lower adsorption capacity in the acidic range is attributed to the competition between excess H^+ ions and the dye cation for the available adsorption sites (Ren *et al.*, 2016). The increase in MG uptake at higher pH values may also be attributed to two reasons: the dimerization of MG or the reaction of MG with sodium hydroxide (Shawabkeha, and Tutunji, 2003). According to Felix (2017), the reaction of MG with sodium hydroxide causes fading of MG. The author attributes the fading to the attack of OH^- on the central C atom of the planar ring system of MG.

The effect of solution pH can also be described based on the zero point of charge (pH_{ZPC}) which is an indication of the ability of the adsorbent surface to become protonated (positively charged) or deprotonated (negatively charged). Jordanian's pH_{ZPC} diatomite was determined and found to be around 5.4. When the pH of the solution is < pH_{ZPC}, the adsorbent surface acquires a positive charge and vice versa (Benmaamar *et al.*, 2016). Therefore, in the alkaline range, the pH of the solution is > pH_{ZPC} and the diatomite acts as a negative surface and enhances the uptake of the positively charged dye (MG). Diatomite shows 16.7-98.9% of MG removal over the whole concentration range (100-900 ppm).

2.1.3 Effect of Particle Size

The particle size is another important factor that affects the adsorption process. To explore the impact of diatomite particle size on the adsorption capacity of MG, multiple adsorption tests were conducted with three different particle sizes namely, 125-250µm, 250-500µm and 500-710µm, where all other factors were kept constant, and the results are shown in **Figure 4**. It is clear from the figure that an inverse relationship exists between diatomite particle size and diatomite adsorption capacity. With the initial MG concentration of 700 (mg/dm^3), MG uptake has increased from 588.9 (mg/g) to 659 (mg/g) as the particle size decreases from 500-710µm to size 125-250µm. This can be explained by the fact that on decreasing the particle size, more surface area is available for the adsorption of MG (Erdem *et al.*, 2005, Joseph *et al.*, 2013). The removal efficiency of MG dropped from 92.1 to 81.1% with increasing particle size from 125-250µm to 500-710µm. Thus, smaller particle size is favorable for the adsorption of MG onto Jordanian diatomite.

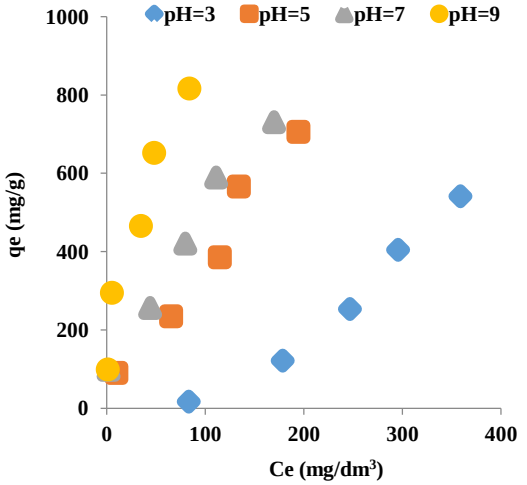

Fig. 3 Effect of the solution pH on the adsorption of MG onto diatomite. Volume of dye solution=25 mL, mass of adsorbent=0.025 g, concentration=100-900 mg/dm^3, particle size=500-710µm, temperature =25^{o}C.

2.2 Adsorption Isotherm Modelling

Equilibrium isotherm models can provide substantial information regarding the capacity of adsorbent, interaction between an adsorbent and adsorbate, surface properties and affinity of the adsorbent and sorption mechanism that can be used for designing the adsorption process (Lee *et al.*, 2018; Sawasdee and Watcharabundit, 2015). Thus, best-fit isotherm is essential. According to Lee *et al.* (2018) fitting the experimental data to different isotherm models is helpful in indicating the most appropriate model to be used in the design of the adsorption system.

Experimental data were analyzed according to the linear form of Langmuir, Freundlich, Temkin, Flory-Huggins, Halsey, and Jovanovic isotherm models and plots were constructed. **Table 1** displays the results of the calculated isotherm constants at pH =7. Langmuir plots gave nonlinear relationships between C_e/q_e and C_e which indicates the inability of the model to simulate the experimental data. However, the experimental data were well fitted with the Freundlich model and this might indicate the heterogeneous distribution of the active sites and

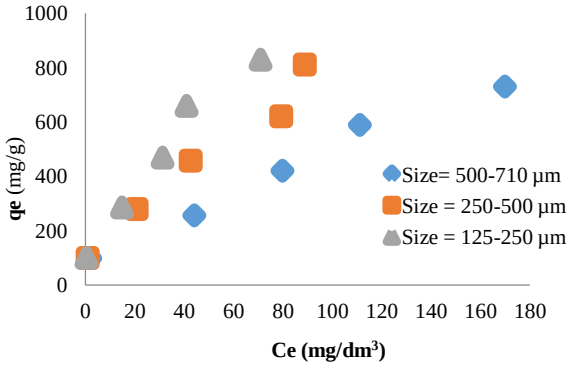

Fig.4 Effect of adsorbent particle size on the adsorption of MG onto diatomite. Volume of dye solution=25ml, mass of adsorbent=0.025g, concentration=100-900 mg/dm^3, pH=7, temperature=25^{o}C.

multilayer adsorption. The Temkin model showed poor representation of the experimental data. The inability of the Temkin isotherm model to simulate the experimental MG data very well may suggest the nonuniform surface morphology of diatomite (Amin *et al.*, 2017). Moreover, it may indicate that the sorbate-adsorbate interactions do not exist. Adsorption energy, ΔQ=(−ΔH), is positive for all studied conditions, indicating the exothermic nature of the adsorption process of MG onto diatomite (Hamdaouia and Naffrechoux, 2007). According to Amin *et al.* (2015), Temkin model is not appropriate for predicting the equilibrium in the complex liquid-phase adsorption systems. The values of the standard Gibbs free energy calculated from the Flory-Huggins model were negative for all the studied conditions, referring to the spontaneity of the adsorption of MG onto Jordanian diatomite and supports an exothermic nature (Theivarasu and Mylsamy, 2011). It is noticeable from Table 1 that the experimental results obtained for MG shows compatible trends with Halsey isotherm. Halsey model supports the Freundlich model and affirms the fact that the adsorption process of MG onto Jordanian diatomite is of a multilayered nature and confirms the heterogeneous nature of diatomite. Sampranpiboon *et al.* (2014) declared that the ability of the Halsey model to fit the experimental data attest to the heterosporous nature of adsorbent. Jovanovic model could not describe the experimental data. This emphasizes that the adsorption of MG onto Jordanian diatomite favors multilayer coverage and again support the assumptions of the Freundlich model. In addition, Table 1 reveals that the correlation coefficient, r^2, for Langmuir model is the lowest. Low values of r^2 indicate the inconsistency of the Langmuir model to fit the experimental data. This was expected since the experimental isotherms obtained did not present the typical Langmuirian form. The correlation coefficient for the Freundlich model was comparatively the highest suggesting the applicability of the Freundlich model to describe the MG-diatomite adsorption process.

Table 1 Isotherm constants for MG-diatomite system at pH = 7 and particle size = 500-710 μm.

Model (Reference)	Linear Form			Constants		r^2
Langmuir (Sampranpiboon *et al.*, 2014)	$\frac{C_e}{q_e}=\frac{1}{K_L}+\frac{a_L}{K_L}C_e$	k_L (dm^3/g)	14.08	R_L	0.073	0.729
Freundlich (Yang *et al.*, 2017)	$Lnq_e=LnK_F+\frac{1}{n}LnC_e$	k_f ($mg/g.(mg/dm^3)^{1/n}$)	67.76	n	2.320	0.941
Temkin (Hamdaouia and Naffrechoux, 2007)	$\theta=\frac{RT}{\Delta Q}LnK_T+\frac{RT}{\Delta Q}LnC_e$	K_T (dm^3/mg)	0.772	ΔQ (kJ/mol)	25.63	0.764
Flory-Huggins (Theivarasu and Mylsamy, 2001)	$Ln\left(\frac{\theta}{C_o}\right)=LnK_{FH}+n\ln(1-\theta)$	K_{FH} (dm^3/mol)	$2.90*10^{-4}$	n	-0.900	0.885
Halsey (Amin *et al.*, 2015)	$Lnq_e=\frac{1}{n_H}LnK_H-\frac{1}{n_H}LnC_e$	K_H (mg/dm^3)	$5.73*10^{-5}$	n	-2.315	0.941
Jovanovic (Sampranpiboon *et al.*, 2014)	$Lnq_e=Lnq_{max}-K_jC_e$	K_J (dm^3/g)	-0.012	q_{max} (mg/g)	130	0.803

Since modeling results manifest that the Freundlich isotherm model is the best one to simulate the adsorption of MG onto diatomite, discussion will be focused more on this model. **Table 2** displays the results of the calculated Freundlich isotherm constants at different pH values. The results also show that the value of n is greater than unity indicating that the MG is favourably adsorbed by diatomite. Yildiz (2017) announced that n value greater than 1 indicates spontaneous adsorption conditions. An increase in K_f values was observed which indicates that adsorption affinity increases with increasing solution pH. This trend may indicate multilayer adsorption. The magnitude of the Freundlich constant indicates easy uptake of MG from aqueous solution. This is in great agreement with the previous findings regarding pH effect on the adsorption of MG. According to Arivoli *et al.* (2009) physisorption is much more favorable when n is less than one. Heydaria and Khavarpour (2018) reported that a higher value of K_f is an indication of a higher affinity of adsorbent toward adsorbate. **Figure 5** displays a theoretical plot of Freundlich isotherm with the experimental data for the adsorption of MG onto diatomite at pH=3. It is obvious from the figure that the experimental data are best fitted with Freundlich isotherm. **Table 3** lists the results of the calculated Freundlich isotherm constants at different particle sizes for MG-diatomite systems. As seen from the table, the Freundlich model again represents the experimental data very well. The values of the correlation coefficient, r^2, for Freundlich model support this finding. It is also evident that the affinity of the adsorbents decreases as the particle size increases. This confirms that MG uptake was a function of the external surface area of the adsorbent. This is consistent with the previous results obtained.

Table 2 Freundlich isotherm constants for the diatomite-MG system at different pH values.

pH	**Freundlich Constants**		
	k_f **($mg/g.(mg/dm^3)^{1/n}$)**	**n**	r^2
3	1.012	1.013	0.996
5	17.49	1.475	0.995
7	67.76	2.320	0.941
9	108.6	2.200	0.964

2.3 Error Analysis

Error function namely, the Average Relative Error Deviation (ARED) and Chi-square test (χ^2) were used to evaluate the fit of the isotherm equations to the experimental data and determine the best- fitting equation. The expression of these error functions are given in Eq. (3) and Eq. (4) (Benmaamar *et al.*, 2016; Kooh *et al.*, 2016):

$$ARED = \frac{100}{n}\sum_{i=1}^{n}\left|\frac{q_{e,\exp} - q_{e,calc}}{q_{e,\exp}}\right|_i \quad (3)$$

and

$$Chi-squareTest\,(\chi^2) = \sum_{i=1}^{n}\frac{(q_{e,\exp} - q_{e,calc})^2}{q_{e,\exp}} \quad (4)$$

Where $q_{e,exp}$ is the experimental value, $q_{e,calc}$ is the calculated value and n is the number of data points in the experiment. The results of these statistical tools showed that the Chi-square test value and ARED value of Freundlich is the smallest. This indicates that the calculated value of q_e using Freundlich model is closer to q_e obtained experimentally. This is consistent with the previous results and manifests the earlier findings that the experimental data are best fitted with Freundlich isotherm. **Table 4** summarizes the results for the adsorption of MG onto diatomite at pH=9.

Table 3 Freundlich isotherm constants for the diatomite-MG system at different particle sizes.

Size (µm)	k_f (mg/g.(mg/dm^3)$^{1/n}$)	n	r^2
125-250	133.5	2.557	0.947
250-500	97.72	2.358	0.959
500-710	67.76	2.320	0.941

Table 4 Error deviation data for the adsorption of MG onto diatomite at pH =9.

Error Function / Isotherm Model	ARED	χ^2
Langmuir	21.73	92.22
Freundlich	11.14	28.91
Temkin	15.35	55.23
Halsey	11.32	29.12
Jovanovic	86.74	163.5

Conclusions

The focus of this research was to investigate the potential use of Jordanian diatomite as an adsorbent for the removal of malachite green dye (MG) from aqueous solution. The results indicated the major role played by the pH of MG solution. The optimum pH value for the removal of MG was = 9. Diatomite particle size showed a vital effect on the adsorption capacity of diatomite and it can be concluded that smaller diatomite particles are recommended for the removal of MG from aqueous solution. Initial MG concentration proved to play an essential role in the adsorption process, the lower the initial dye concentration, the faster the MG removal. Freundlich isotherm was able to simulate the equilibrium data very well. Based on these mentioned results, Jordanian diatomite could potentially be used as a low-cost promising adsorbent for treating MG effluents.

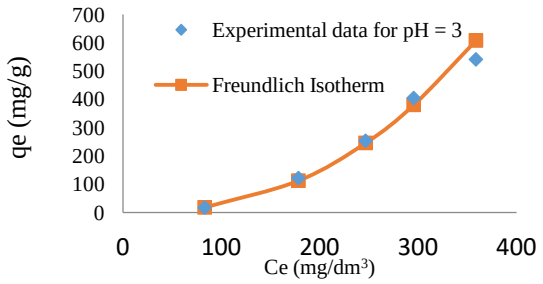

Fig. 5 Model fit of adsorption isotherm of MG adsorption onto diatomite

Nomenclature

a_L	=Langmuir constant	[dm^3/mg]
C_e	=Equilibrium dye concentration	[mg/dm^3]
C_o	=Initial dye concentration	[mg/dm^3]
K_F	=Freundlich constant	[mg/g.(mg/dm^3)$^{1/n}$]
K_{FH}	=Equilibrium constant	[dm^3/mol]
K_H	=Halsey isotherm constant	[mg/dm^3]
K_L	=Langmuir constant	[dm^3/g]
K_J	=Jovanovic constant	[dm^3/g]
K_T	=Equilibrium binding constant	[dm^3/mg]
m	=Mass of the diatomite	[g]
n	=Heterogeneity factor	[-]
n_H	=Halsey isotherm constant	[-]
ΔQ	=Variation of adsorption energy	[J/mol]
q_e	=Amount of MG adsorbed at equilibrium	[mg/g]
$q_{e,calc}$	=Calculated value	[mg/g]

$q_{e,exp}$	=Experimental value	[mg/g]
q_{max}	=Maximum uptake of adsorbate	[mg/g]
R	=Universal gas constant	[J/mol.K]
T	=Absolute temperature	[K]
V	=Volume of MG solution	[dm^3]
θ	=Fractional coverage	[-]

References

Alali, J., Diatomite**,** Ministry of Energy and Mineral Resources, Jordan (2015).

Al-Degs, Y. S. Adsorption of Anionic Reactive Dyes on Activated Carbon from Aqueous Solution [dissertation]. Queen's University Balfast. 2000.

Al-Degs, Y., Tutunji M, and Shawabkeha R., "The Feasibility of Using Diatomite and Mn–Diatomite for Remediation of Pb^{2+}, Cu^{2+}, and Cd^{2+} from Water", *Sep. Sci. & Tech*., **35**, 2299–2310 (2000).

Al-Wahbi, A., "Adsorption of Diazo Dye C.I. Acid Red 97 from Aqueous Solution onto Yemen Natural Clay: Equilibrium and Thermodynamic Studies", *Jordanian J. of Eng. Chem. Indus. (JECI)*, **1**, 1-11 (2018).

Ali, I., Peng C., Yeac T., and Naz, I. "Sorption of Cationic Malachite Green Dye on Phytogenic Magnetic Nanoparticles Functionalized by 3-Marcaptopropanic Acid", *Royal Soci. Chem. Adv.*, **8**, 8878–8897 (2018).

Alkan, S., Çalişkan M., Irende I., and Kul A., "Adsorption Equilibrium and Thermodynamics of Diatomite (Çaldiran/Van) On Some Textile Dyes", *J. Chem. Soc. Pakistan*, **40**, 457-466 (2018).

Amin, M., Alazba A., and Shafiq M., "Adsorptive Removal of Reactive Black 5 from Wastewater Using Bentonite Clay: Isotherms, Kinetics and Thermodynamics", *Sustainability*, **7**, 15302-15318 (2015).

Amin, M., A. Alazba A., and Shafiq M., "Non-Spontaneous and Multilayer Adsorption of Malachite Green Dye by Acacia Nilotica Waste with Dominance of Physisorption", *Water Sci. and Tech.*, **76**, 1805-1815 (2017).

Arivoli, S., Hema M., and M. Prasath P., "Adsorption of Malachite Green onto Carbon Prepared from Borassus Bark", *The Arabian J. Sci, Eng.*, **34**, 31-42 (2009).

Benmaamar, Z., H. Boutoumi, H. Hamitouche, H. Benmaamar, S. Mazari, A. Benmaamar and A. Aggoun, "Simulation of Adsorption Kinetics of Malachite Green onto Coffee Residues", *Revue Science des Matériaux, Laboratoire*, **8**, 1-11 (2016).

Blanco-Flores, A., Gutiérrez-Segura E., Sánchez-Mendieta V., and Vilchis-Néstor, A. "Removal of Malachite Green Dye from Aqueous Solution Through Inexpensive and Easily Available Tuffite, Bentonite and Vitreous Tuff Minerals"**,** *Revista Latinoamericana de Recursos Naturales*, **12**, 1-17 (2016).

Chowdhury, S. and Saha, D. "Adsorption of Malachite Green from Aqueous Solution by NaOH-Modified Rice Husk: Fixed-Bed Column Studies", *Envi. Prog. and Sust. Energy*, **32**, 633-639 (2013).

Dhahir, S. A., Abdul-Hussein E., Sarhan S., and Faraj N., "Adsorption of Malachite Green Dye From Aqueous Solution onto Iraqi Raw Al-Hussainiyat Clay", *Eur. Chem. Bull.*, **2**, 866-872 (2013).

Erdem, E., Çölgeçen G., and Donat R., "The Removal of Textile Dyes by Diatomite Earth", *J. Collo. and Interf. Sci.*, **282**, 314–319 (2005).

Felix, L., "Kinetics of the Reaction between Malachite Green and Hydroxyl Ion in the Presence of Reducing Sugars", *J. Chem. Tech. and Metal.*, **52**, 526-531 (2017).

Gajare, S. M. and Menghani, S. "Biosorption of Malachite Green by Naturally Grown Algal Biomass from Girna River, Jalgaon District, Maharashtra", *J. Algal Biomass Utln.*, **3**, 60–65 (2012).

Hamdaouia, O. and Naffrechoux, E. "Modeling of Adsorption Isotherms of Phenol and Chlorophenols onto Granular Activated Carbon Part I. Two-Parameter Models and Equations Allowing Determination of Thermodynamic Parameters", *J. Haz. Mat.*, **147**, 381–394 (2007).

Heydaria, R. and Khavarpour, M. "Adsorption of Malachite Green from Aqueous Solution by Nanozeolite Clinoptilolite: Equilibrium, Kinetic and Thermodynamic Studies", *Int. J. Eng.*, **31**, 1-11 (2018).

Joseph, F., Agrawal Y., and Rawtani, D. "Behavior of Malachite Green with Different Adsorption Matrices", *Frontiers in Life* Sci., **7**, 99-111 (2013).

Khraisheha, M., A. Al-Ghouti M., Allen S., and Ahmad, M. "Effect of OH and Silanol Groups in the Removal of Dyes from Aqueous Solution Using Diatomite", *Water Res.*, **39**, 922–932 (2005).

Kooh, M., Dahri M., M. and Lim, L. "The Removal of Rhodamine B Dye from Aqueous Solution Using *Casuarina Equisetifolia* Needles as Adsorbent" *Cogent Envi. Sci*., **2**, 1-14 (2016).

Lai, C. H. and C. Y. Chen, "Removal of Metal Ions and Humic Acid from Water by Iron-Coated Filter Media", *Chemosphere***,** **44**, 1177-1184 (2001).

Lee, Y., Amini M., Sulaiman N., Mazlan M., and Boon, J. "Batch Adsorption and Isothermic Studies of Malachite Green Dye Adsorption Using *Leucaena Leucocephala* Biomass as Potential Adsorbent in Water Treatment", *Songklanakarin J. Sci. Technol.*, **40**, 563-569 (2018).

Litefti, K., Freire, M., Stitou M., and González-Álvarez J. "Biosorption of cationic textile dyes by a forest industry residue: *Pinus pinaster* bark", *15th International Conference on Environmental Science and Technology*, Greece: 2017.

Oktay, B., Elevli S., and Coruh, S. "Malachite Green Dye Removal Using Montmorillonite Clay: Full Factorial Design Analysis", *Int. J. Adv. Sci. Eng. Tech.*, **4**, 13-17 (2016).

Pan, X. and Zhang, D. "Removal of Malachite Green from Water by *Firmiana Simplex* Wood Fiber", *Elect. J. Biotech*., **12**, 4-14 (2009).

Pragathiswaran, C., Krishnan N., Abbubakkar, B., Govindhan P., and Abuthahir K., "Adsorption of Malachite Green Dye onto Activated Carbon Obtained from the Gloriosa Superba Stem", *Int. J. Res. Phar. Chem*., **6**, 57-61 (2016).

Ren, Z., Guan, J., Gao, H., Tian, J., Wen Y., and Zheng, R. "Characteristics of Cationic Red X-Grl Adsorption by Raw Diatomite and Diatomite Concentrate", *Physicochem. Probl. Miner. Process*, **52**, 44−55 (2016).

Roja, K., Ramesh N., and Ramesh. S., Adsorption Studies for the Removal of Malachite Green Dye from Aqueous Solution Using Graphene Oxide. International Conference on Recent Trends in Environmental Science and Engineering, India: 2017.

Salman, T., Temel, F., Turan N., and Ardali, Y. "Adsorption of Lead (Ii) Ions onto Diatomite from Aqueous Solutions: Mechanism, Isotherm and Kinetic Studies", *Global NEST J.*, **18**, 1-10 (2016).

Sampranpiboon, P., Charnkeitkong P., and Feng, X. "Equilibrium Isotherm Models for Adsorption of Zinc (II) ion from Aqueous Solution on Pulp Waste", *Wseas Trans. on Envir. Devel.*, **10**, 35-47 (2014).

Sartape, A., M. Mandhare, A., Jadhav, V., Raut, P., Anuse M., and Kolekar, S. "Removal of Malachite Green Dye from Aqueous Solution with Adsorption Technique Using Limonia Acidissima (Wood Apple) Shell as Low Cost Adsorbent", *Arabian J. chem*.,**10**, S3229-S3238 (2017).

Sawasdee, S. and Watcharabundit, P. "Equilibrium, Kinetics and Thermodynamic of Dye Adsorption by Low-Cost Adsorbents", *Int. J. Chem. Eng. Appl.*, **6**, 444-449 (2015).

Shawabkeha, R., and Tutunji, M. "Experimental study and modeling of basic dye sorption by diatomaceous clay", *App. Clay Sci.*, **24**, 111–120 (2003)

Theivarasu, C., and Mylsamy, S. "Removal of Malachite Green from Aqueous Solution by Activated Carbon Developed from Cocoa *(Theobroma Cacao)* Shell - A Kinetic and Equilibrium Studies", *E-J. Chem.*, **8**, S363-S371 (2011).

Tian, L., Zhang, J., Shi, H., Li N., and Ping, O. "Adsorption of Malachite Green by Diatomite: Equilibrium Isotherms and Kinetics Studies", *J. Disp. Sci. Tech*., **37**, 1059-1066 (2016).

Yang, X., Zhang, Y., Wang, L., Cao, L., Li. K., and Hursthouse, A. "Preparation of a Thermally Modified Diatomite and a Removal Mechanism for 1-Naphthol from Solution", *Water*, **9**, 651-665 (2017).

Yildiz, S., "Kinetic and Isotherm Analysis of Cu(Ii) Adsorption onto Almond Shell (*Prunus Dulcis*)", *Ecol. Chem. Eng. S*, **24**, 87-106 (2017).

AL-BALQA APPLIED UNIVERSITY

Hashemite Kingdom of Jordan

Scientific Research Support Fund

المجلة الأردنية للهندسة والصناعات الكيميائية

DECEMBER 2019 | VOLUME 02 | ISSUE 03

ISSN 2617 - 720X (Online)
ISSN 2616 - 9584 (Print)

JJECI

www.jjeci.com

info@jjeci.com

مجلة علمية عالمية متخصصة محكمة

تصدر بدعم من صندوق دعم البحث العلمي